ELSEVIER

Contents lists available at ScienceDirect

Science of the Total Environment

journal homepage: www.elsevier.com/locate/scitotenv





Latitudinal gradient and influencing factors of deep-sea particle export along the Kyushu-Palau Ridge in the Philippine Sea

Ziyu Wang ^a, Chen Fang ^c, Chenghao Yang ^d, Guoyin Zhang ^e, Dong Sun ^{a,b,*}

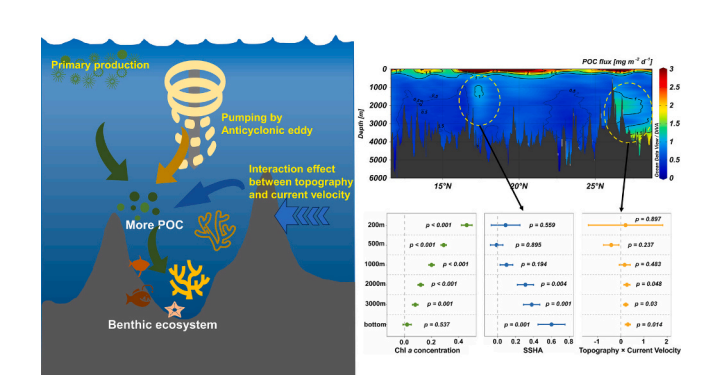
- a Kev Laboratory of Marine Ecosystem Dynamics. Second Institute of Oceanography. Ministry of Natural Resource. Hanezhou 310012. China
- ^b Southern Marine Science and Engineering Guangdong Laboratory (Zhuhai), Zhuhai 519000, China
- ^c College of Oceanography, Hohai University, Nanjing 210024, China
- d State Key Laboratory of Satellite Ocean Environment Dynamics, Second Institute of Oceanography, Ministry of Natural Resources, Hangzhou 310012, China
- e Key Laboratory of Submarine Geosciences, Second Institute of Oceanography, Ministry of Natural Resources, Hangzhou 310012, China

HIGHLIGHTS

• The POC flux along the Kyushu-Palau Ridge was firstly measured by UVP.

- 37 % of POC output from 200 m was preserved to 2000 m in WPWP and up to 51 % in NPSG.
- Near-bottom POC fluxes north of 25°N significantly higher than the entire transect.
- POC fluxes influenced by chlorophyll, eddy, current velocity, and topography

GRAPHICAL ABSTRACT



ARTICLE INFO

Editor: Olga Pantos

Keywords:
POC flux
Mesoscale eddy
Resuspension
Warm pool
Benthic community
Habitat classification

ABSTRACT

The export of particulate organic matter (POM) to deep-sea is crucial for deep-sea ecosystems. However, *in situ* measurements of large-scale POM export flux are scarce in the tropical and subtropical western Pacific, leading to reliance on biogeochemical models or sediment trap data from a few stations. To address this gap, the underwater vision profiler was used to measure particulate density and to calculate particulate organic carbon (POC) fluxes along the Kyushu–Palau Ridge (KPR) in the Philippine Sea. The results revealed a significant latitudinal gradient of POC fluxes: 37 % of the POC output from 200 m depth was preserved to 2000 m in the Western Pacific Warm Pool and up to 51 % was preserved in the North Pacific Subtropical Gyre. The near-bottom POC fluxes north of 25° N (1.64 ± 0.80 mg m $^{-2}$ d $^{-1}$) were significantly higher than the average near-bottom value of the entire transect (0.60 ± 0.43 mg m $^{-2}$ d $^{-1}$). Multiple linear regression analysis showed that the chlorophyll concentration had a significant positive effect on the POC fluxes at all depths, except near the bottom, while local factors such as mesoscale eddies and the interaction effect between the topography and current velocity only had significant effects on the POC fluxes at depths of >2000 m. Particle size spectrum analysis revealed that particles ranging from 64 to 323 μ m in size exerted a dominant influence on the increase in the POC fluxes in the near-

E-mail address: sund@sio.org.cn (D. Sun).

^{*} Corresponding author at: Key Laboratory of Marine Ecosystem Dynamics, Second Institute of Oceanography, Ministry of Natural Resource, Hangzhou 310012, China.

bottom layers situated north of 25° N. These findings indicated that the spatial heterogeneity of POC fluxes in the western Pacific was governed not only by upper ocean primary productivity but also by mesoscale processes, current velocity, and topography. These results provided crucial fundamental information for cartography of the distribution and simulation of the dynamics of deep-sea organisms along the KPR in the Philippine Sea.

1. Introduction

Biotic carbon pumps transport 5-20 Gt of carbon annually from the surface to the deep ocean, and sinking organic matter is one of the major ways in which carbon is transferred downwards. These particles have diameters of several micrometers to several centimeters, and particles with diameters of >0.5 mm are known as marine snow (Alldredge and Silver, 1988). These particles sink into the deep sea and provide an essential food source for deep-sea biomes, including benthic organisms and demersal fish (Baltar et al., 2009; Turner, 2015). This food supply from the upper layers of the ocean is one of the main drivers of the spatial and temporal variations in deep-sea ecosystems. On the global scale, patterns of benthic biomass are positive functions of the particulate organic matter (POM) supplied to the benthos from the upper layers (Wei et al., 2010). At the regional scale, this pattern is still widespread. Tittensor et al. (2011) showed that in the North Atlantic, POC fluxes have the greatest potential impact on deep-sea molluscan diversity. Wolff et al. (2011) also showed that the timing, quantity, and quality of POM export strongly influence the deep-sea benthic community structure in the Southern Indian Ocean. A long time series study in the NE Pacific revealed that climate-induced interannual fluctuations in POC fluxes cause interannual fluctuations in benthic megafauna abundance, but this has a certain time lag (Ruhl and Smith, 2004). In addition, the vital activity of mesopelagic organisms is also largely supported by sinking POC fluxes (Arístegui et al., 2002). Furthermore, changes in POC fluxes not only affect the community level but also control ecosystem functions, and in the North Pacific, seasonal fluctuations in the sediment community oxygen consumption exhibit a pattern that is more or less consistent with that of the POC fluxes (Gooday, 2002).

The assertion that the export flux of POC mirrors the primary productivity pattern in the upper ocean has been widely acknowledged (Lins et al., 2014). Recent estimates indicate that the net primary productivity (NPP) of marine phytoplankton is approximately 50 Pg C year⁻¹, and 10-20 % of the NPP is exported from the upper ocean into the mesopelagic layer as POC (Bisson et al., 2020). Nevertheless, certain local and/or abrupt oceanographic events can disrupt these associations. For example, the 1991-1992 ENSO event resulted in a mismatch between the primary productivity and 150 m layer POC fluxes, which was observed in a 5-year time series study conducted at ALOHA station (Karl et al., 1996). Analysis of the seasonal production-flux revealed that there is significant variability in the vertical transport efficiency of POC fluxes, particularly during algal bloom production, during which the ratio of the POC flux to the primary productivity is typically half of the annual mean (Lutz et al., 2007). Additionally, mesoscale eddies play a role in influencing POC fluxes by driving periodic enhancement of the vertical organic carbon export to the mesopelagic zone through localized increases in the primary productivity (Lévy et al., 1998) and enhanced vertical velocities associated with eddy perimeters and fronts (Van Haren et al., 2006). Mesoscale eddies can trap POC-rich coastal upwelling water and transport it to the pelagic region (Amos et al., 2019). Although anticyclonic eddies do not contribute as much to the offshore transport of coastal waters as cyclonic eddies, an increase in the POC flux in the core of anticyclonic eddies has also been observed (Zhou et al., 2013). Shih et al. (2015) further confirmed that anticyclonic eddies in subtropical oligotrophic waters can increase carbon export fluxes and that the edges of eddies are important channels for carbon sequestration in deeper water. The interaction of the seafloor topography with the hydrodynamic environment is also an important factor. Jiang et al. (2021) showed that density fronts and rapids-induced

resuspension in the boundary layer at the base of seamounts can lead to increased POC fluxes. Misic et al. (2012) also recorded an increase in organic matter due to sediment deposition and resuspension along slopes/flanks in the mesopelagic layer. In addition, typhoons (Hung et al., 2009; Siswanto et al., 2007), ocean fronts (Ohman et al., 2012), and the community structure and behavior of zooplankton (Al-Mutairi and Landry, 2001) can also have significant effects on POC fluxes.

The current tools used to measure POC fluxes include radioisotope methods (Zhou et al., 2020), sediment trap methods (Buesseler et al., 2007a), in-situ optical measurements (Kiko et al., 2017), and remote sensing methods (Allison et al., 2010). In-situ optical devices are small enough to be mounted on conductivity, temperature, and depth (CTD)rosette samplers and small uncrewed platforms such as underwater gliders (Picheral et al., 2022) and can provide greater spatial coverage in the open ocean than traditional techniques such as sediment traps (Giering et al., 2020). High resolution in-situ optical imaging systems can be combined with image processing techniques for particle identification, describing the particle abundance, size, and type and thus the source and formation of the particles. The underwater vision profiler (UVP) is one type of in-situ optical device. Over the past decade, data from UVPs have contributed to a better understanding of particle and plankton dynamics in the ocean (Guidi et al., 2015; Ramondenc et al., 2016; Stemmann et al., 2008a, b). Optical methods, represented by UVPs, are well suited to studying patterns of large-scale POC fluxes in the ocean. The results of such studies are in good agreement with the results from sediment traps. For example, Stemmann et al. (2000) used particulate matter and zooplankton distribution data collected using a UVP during a time-series cruise in the NW Mediterranean to study the diurnal variability in the size distribution of >0.15 mm particles. Stemmann et al. (2008a) analyzed the number and volume distribution of large (d $> 100 \mu m$) particles using UVP over a 7500 km transect through the South Pacific Gyre. Guidi et al. (2008) linked in situ particle data from a UVP to sediment trap data and proposed a simple power relationship to estimate the particle mass, particulate organic nitrogen (PON), and POC fluxes, providing a quantitative basis for the estimation of particle fluxes and POC fluxes in the ocean using UVP data. Kiko et al. (2017) measured multi-particle size particle profiles using a UVP in the equatorial Atlantic and Pacific oceans and provided the first systematic mapping of POC fluxes in the global equatorial ocean based on these data. Gillard et al. (2022) determined particle abundance and size distributions across the Clarion-Clipperton Zone water column using a UVP.

As the largest marginal sea in the Western Pacific Ocean, the Philippine Sea is divided into two sections by the Kyushu-Palau Ridge (KPR). The KPR extends north-south across the entire Philippine Sea and has complex and rugged topography, including many seamounts and troughs (Ding et al., 2022; Qin et al., 2021). The dominant environmental gradients in the Philippine Sea are reflected in several aspects such as the temperature, primary productivity, topography, eddies, and currents. The temperature gradient increases with decreasing latitude, with surface temperatures in the southern Western Pacific Warm Pool (WPWP) reaching >28 °C (Hu et al., 2020). A previous study along the 137°E transect has shown that there is a latitudinal gradient in the chlorophyll concentration and productivity-related plankton biomass (Sugimoto and Tadokoro, 1998). A similar pattern was also confirmed by phytoplankton community structure data along the 141°E transect (Girault et al., 2016). The Philippine Sea is controlled by several major currents in the epipelagic zone, including the North Equatorial Current (NEC), the North Equatorial Counter Current (NECC), and the Kuroshio Current, which weakly fluctuate seasonally, resulting in a relatively stable latitudinal zonation (Hu et al., 2015), with the WPWP dominating in the south, the North Pacific Subtropical Gyre (NPSG) dominating in the center and north and the transition zone and Kuroshio-influenced zone north of 30°N (Girault et al., 2016; Longhurst, 2007). Previous studies on the POC flux were dominated by sediment trap studies. Kawahata et al. (2000) used sediment trap data to compare the POC fluxes and primary productivity in the western and central eastern WPWP. Honda et al. (2016) conducted floating sediment trap experiments at station S1 in different seasons to characterize the sinking of particulate matter in the upper 200 m of the subtropical northwestern Pacific water column. On a larger scale, the latitudinal gradient of particulate matter export in the Philippine Sea and its relationship to environmental gradients is unclear.

The KPR has been designated as an ecologically or biologically significant marine area (EBSA) by the Convention on Biological Diversity, mainly due to the importance of its complex topography for potential high deep-sea biodiversity (CBD, 2016) although many key environmental contexts, including gradients in the food supply of deep-sea ecosystems (Lampadariou and Tselepides, 2006), have been completely unknown until now. In this study, in situ optical data from a UVP along the KPR were used to estimate the POC fluxes on a large scale and to investigate the potential mechanisms of the variation in the POC fluxes at different depths. Therefore, the results of this study improve our understanding of the large-scale spatial patterns of deep-sea POC fluxes and provide key data for characterizing and mapping benthic biodiversity along the KPR.

2. Materials and methods

2.1. Data collection

From 27 October to 15 November 2021, a survey was conducted during the COMRA DY68 cruise in the Philippine Sea (Fig. 1), with nineteen stations distributed in a transect over 1900 km long along the Kyushu-Palau Ridge at latitudes of 11–29°N and longitudes of 134–138°E. The study area was divided into two zones at 20°N based on differences in the water masses (Hu et al., 2015) and temperature profile (Fig. 2a): the NPSG and the WPWP. In the WPWP zone, stations S09–S12 were influenced by an anticyclonic eddy. Particle size and abundance data were collected in the full depth range using a high resolution, high frequency underwater vision profiler (UVP 6.0). The sampling frequency was 20 Hz. The UVP system detected and counted all objects larger than 64 µm within a limited illumination volume of approximately 1 L. The particles imaged by the UVP included all types of particles, from specific particles (e.g., fecal particles) to very complex particles such as

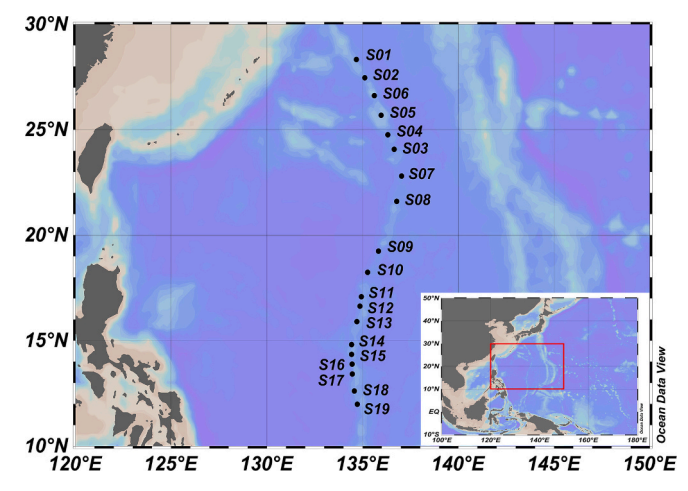


Fig. 1. Station locations along the KPR transect in the Philippine Sea.

aggregates composed of multiple sources (phytoplankton and zooplankton detritus and minerals). In this study, the UVP was mounted on a CTD rosette sampler (SBE 911plus, Seabird Scientific, USA). Temperature, salinity, and chlorophyll concentration were recorded by the CTD system, and the chlorophyll concentration was converted from fluorescence values *via* real calibration.

The current velocity was simulated using the hybrid coordinate ocean model (HYCOM) (Bleck, 2002; Halliwell et al., 1998, 2000). In this study, Version 3.1 assimilated data were used to interpret the high near-bottom anomalies along the KPR, and the model resolution was 1/ 12°. The HYCOM is a primitive equation ocean general circulation model that evolved from the Miami isopycnic-coordinate ocean model (MICOM) developed by Rainer Bleck and colleagues. The HYCOM's vertical coordinates remain isopycnic in the open, stratified ocean, but they transition smoothly to z-coordinates in the weakly stratified upper ocean mixed layer, to terrain-following sigma coordinates in shallow water regions, and back to z-level coordinates in very shallow water. The sea surface height anomaly data were downloaded from the Global Ocean Gridded L4 Sea Surface Heights and Derived Variables Reprocessed 1993 Ongoing dataset (doi:10.48670/moi-00148 and https://data .marine.copernicus.eu/). The bathymetry data for the KPR were collected by the Kongsberg EM124 multi-beam echosounder and the raw data were collected and stored using the SIS software as kmall files. The data were processed using the QPS Qimera software, including motion attitude correction, sound velocity profile correction, and data cleaning, and then, the data were gridded to produce a 50 m grid file. A topographic map was produced from the grid file, and the terrain slope was calculated from the slope of the adjacent water depth.

2.2. Calculation of particle fluxes

The POC flux was calculated using the method proposed by Guidi et al. (2008), which relates sediment trap data to the particle size (d) distribution to estimate the vertical fluxes (F) of the mass and particulate organic carbon (POC) using a simple power relationship $(F = Ad^b)$.

The coefficients (A) and exponents (b) and their associated standard deviations (STD) are given in the text as empirical relationships between the aggregate size and associated mass, POC, particulate inorganic carbon (PIC), and PON fluxes, as determined using the minimization of the flux estimates from the UVP and measurements from the sediment trans.

When calculating F_m (Mass flux), A=109.5, and b=3.52. When calculating F_{poc} (POC flux), A=12.5, and b=3.81.

For the calculation of the POC flux, only the sinking particle category identifiable in the dataset, *i.e.*, 64–1020 μm particulate matter, was retained. The data for particles larger than 1020 μm were removed because particles larger than this size are extremely limited in number and are mostly mesozooplankton, which are not part of the gravity-based sinking particles. To facilitate the differentiation of the contribution of the particles of different sizes to the total POC flux, we categorized the particles into three types based on their particle size: small, including particles with ESDs (equivalent spherical diameter, ESD) of 64–80.6 μm , 80.6–102 μm , 102–128 μm , 128–161 μm , 161–203 μm , 203–256 μm , and 256–323 μm ; medium, including particles with ESDs of 323–406 μm , 406–512 μm , and 512–645 μm ; and large, including particles with ESDs of 645–813 μm and 813–1020 μm .

2.3. Statistical analyses

To investigate the effect of the chlorophyll concentration on the POC fluxes in each water layer, linear fitting and correlation tests were performed using the integrated chlorophyll values (0–200 m) with POC fluxes in each water layer. To analyze the spatial variation in the particle size structure between the 3000 m layer and the near-bottom layer, permutational multivariate analysis of variance (PERMANOVA) was performed in the NPSG and WPWP. To investigate the possible effects of

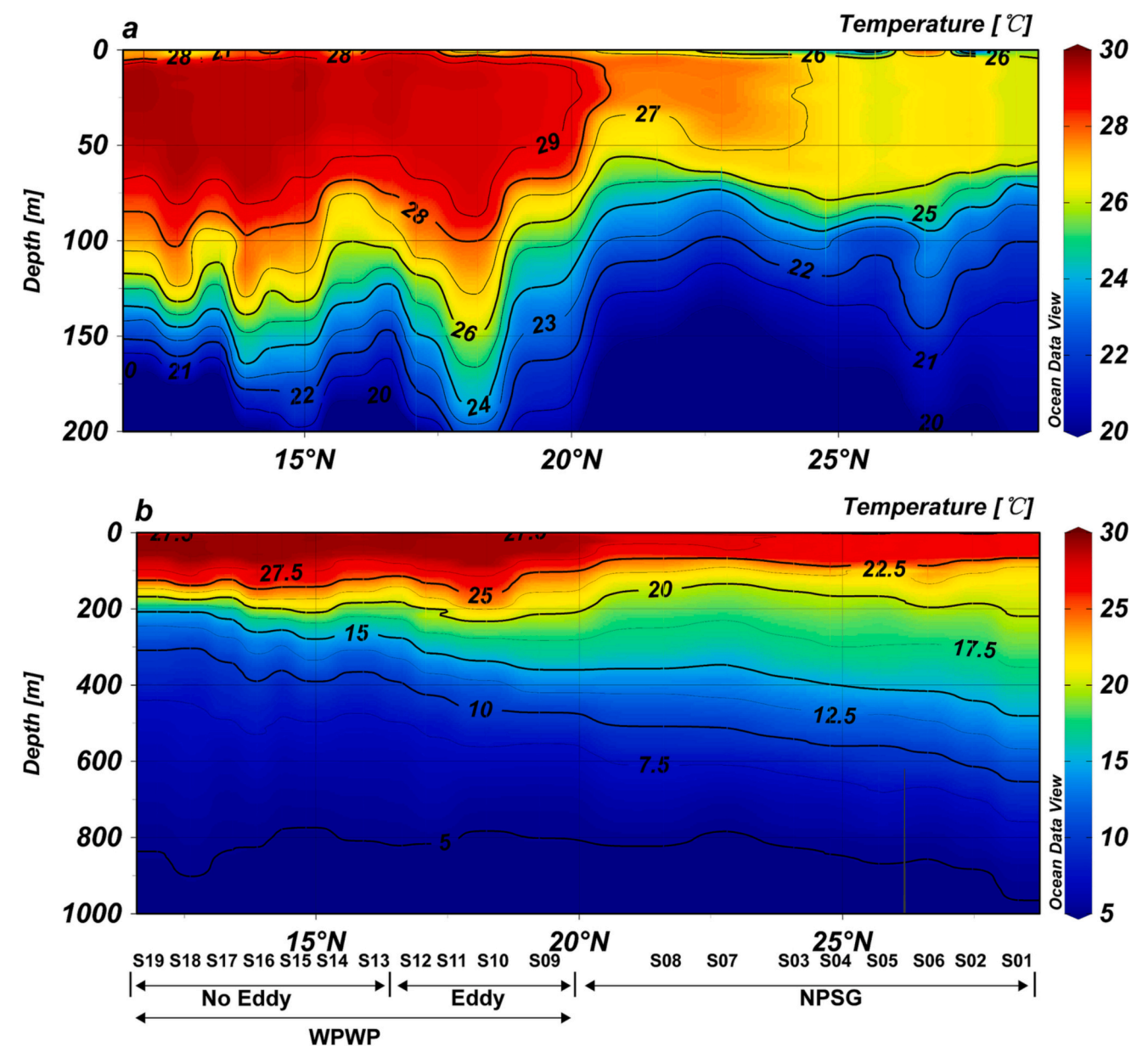


Fig. 2. Vertical distribution of the temperature along the south-north transect along the KPR. (a) 0-200 m; and (b) 0-1000 m.

the chlorophyll concentration, sea surface height anomaly (SSHA), topography, and current velocity on the POC flux, we performed multiple linear regression analyses of the relationships between the POC flux and the chlorophyll concentration, SSHA, and the interaction effect between the topography and current velocity (T-V) to investigate the influences of the environmental parameters. Since there is no direct relationship between one of the individual factors (topography or current velocity) and the POC flux, we only considered the T-V in the multiple linear regression analysis and did not include the two independent factors of the topography and current velocity. The T-V was defined as the multiplication of the topographic factor and the current velocity in this study. The topographic factor was calculated using the vertical depth deviation between the depth of the specific POC flux layer and the depth of the shallowest point on the topography within a 0.5° radius (~ 45 km) of a specific station position. When the former depth was shallower than the latter, which means that the POC flux depth was shallower than the depth of the shallowest surrounding topography, it was assumed that the POC flux at this depth was not influenced by the interaction between the topography and current velocity. In this case,

the topography factor was assigned a value of zero. The original data were standardized and normalized when necessary. Before building the multiple linear regression model, the independent variables were tested for multicollinearity. All of the statistical analyses were conducted in R (version 4.2.0) (R Core Team, 2022).

3. Results

3.1. Temperature and salinity

The main feature of the surface temperature variation along the $135^{\circ}E$ transect was a uniform, monotonic increase from $26.2~^{\circ}C$ in the north to $29.7~^{\circ}C$ in the south (Fig. 2). In the mesopelagic layers, the temperatures in the northern part exceeded those in the southern part, and the isotherm $15~^{\circ}C$ line extended from a depth of 200~m in the south to 400~m in the north. A clear temperature division existed at around $20^{\circ}N$. At stations 508~ and 509, located north and south of $20^{\circ}N$, respectively, there was a distinct temperature gradient, with a maximum surface water temperature of $28.0~^{\circ}C$ and an average temperature of

 $25.8\,^{\circ}\mathrm{C}$ within 100 m of the surface layer at station S08, while at station S09 these values were $29.1\,^{\circ}\mathrm{C}$ and $28.1\,^{\circ}\mathrm{C}$, respectively, and the greatest variation occurred between these stations. The salinity profiles revealed that the stations were hypersaline water masses (<33.5 psu) within 15 m of the surface layer (Fig. 3), and from south to north, the hypersaline zone (>34.75 psu) gradually increased with increasing depth, extending to approximately 200 m in the extreme south and 400 m in the extreme north. There was also a clear divide in the salinity at around $20^{\circ}\mathrm{N}$, with the stations south of $20^{\circ}\mathrm{N}$ having a noticeably lower mean salinity within 100 m of the surface layer (34.0 psu) than the stations north of $20^{\circ}\mathrm{N}$ (34.3 psu). This high temperature, low salinity water mass south of $20^{\circ}\mathrm{N}$ is referred to as the WPWP in this paper.

3.2. Size structure of particles and POC flux

Across the south-north transect, the POC fluxes decreased with increasing depth. The POC fluxes at 200 m, 500 m, 1000 m, 2000 m, 3000 m, and the near-bottom layers were 1.41 \pm 0.31 mg m $^{-2}$ d $^{-1}$, 0.83

 $\pm~0.13$ mg m $^{-2}~d^{-1},~0.65\pm0.15$ mg m $^{-2}~d^{-1},~0.57\pm0.21$ mg m $^{-2}~d^{-1},~0.57\pm0.26$ mg m $^{-2}~d^{-1},~and~0.60\pm0.43$ mg m $^{-2}~d^{-1},~respectively.$ However, the POC fluxes also exhibited region-specific spatial behavior at different depths. In the upper ocean, the regions between 15 and 21°N and near 27°N exhibited high POC fluxes (> 3.0 mg m $^{-2}~d^{-1}).$ At 500–2000 m, the area around 17°N and north of 27°N exhibited high POC fluxes (> 1.0 mg m $^{-2}~d^{-1}).$ At greater depths, high values only occurred in the region north of 27°N, especially near the bottom where the POC fluxes peaked at up to 2.21 mg m $^{-2}~d^{-1}$ (Fig. 4). In addition, the coefficient of variation of the POC fluxes increased with increasing depth across the transect, with values of 0.22, 0.15, 0.23, 0.37, 0.46, and 0.71 at depths of 200, 500, 1000, 2000, 3000 m, and the near-bottom lavers, respectively.

The contribution of each particle size to the total POC flux is shown in Figs. 5 and 6. In general, the small and medium particles were the main contributors to the total POC flux. From a depth of 200 m to the 3000 m layer, the POC flux associated with small particles decreased with increasing depth, and their relative contribution decreased. In

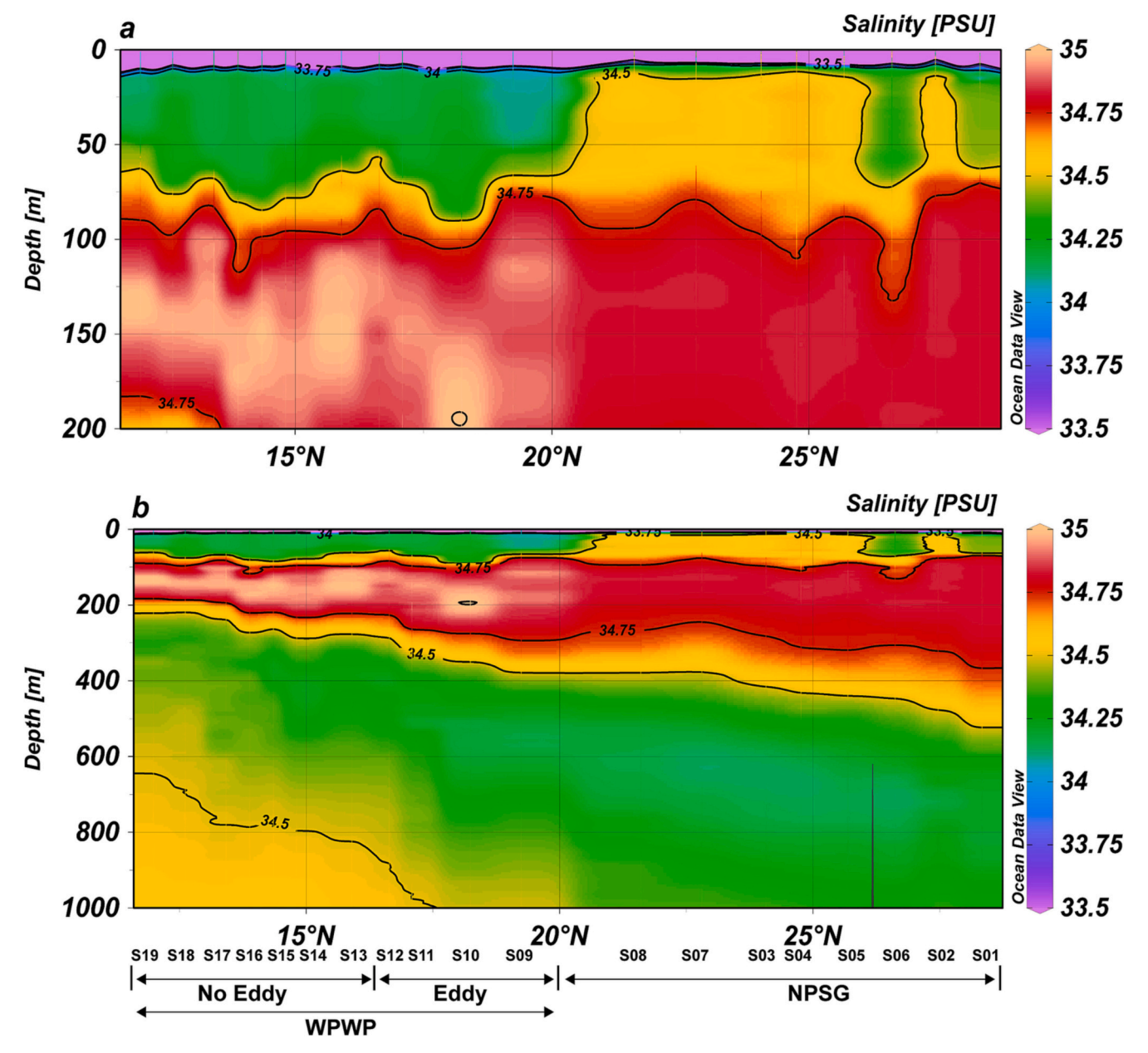


Fig. 3. Vertical distribution of the salinity along the south-north transect along the KPR. (a) 0-200 m; and (b) 0-1000 m.

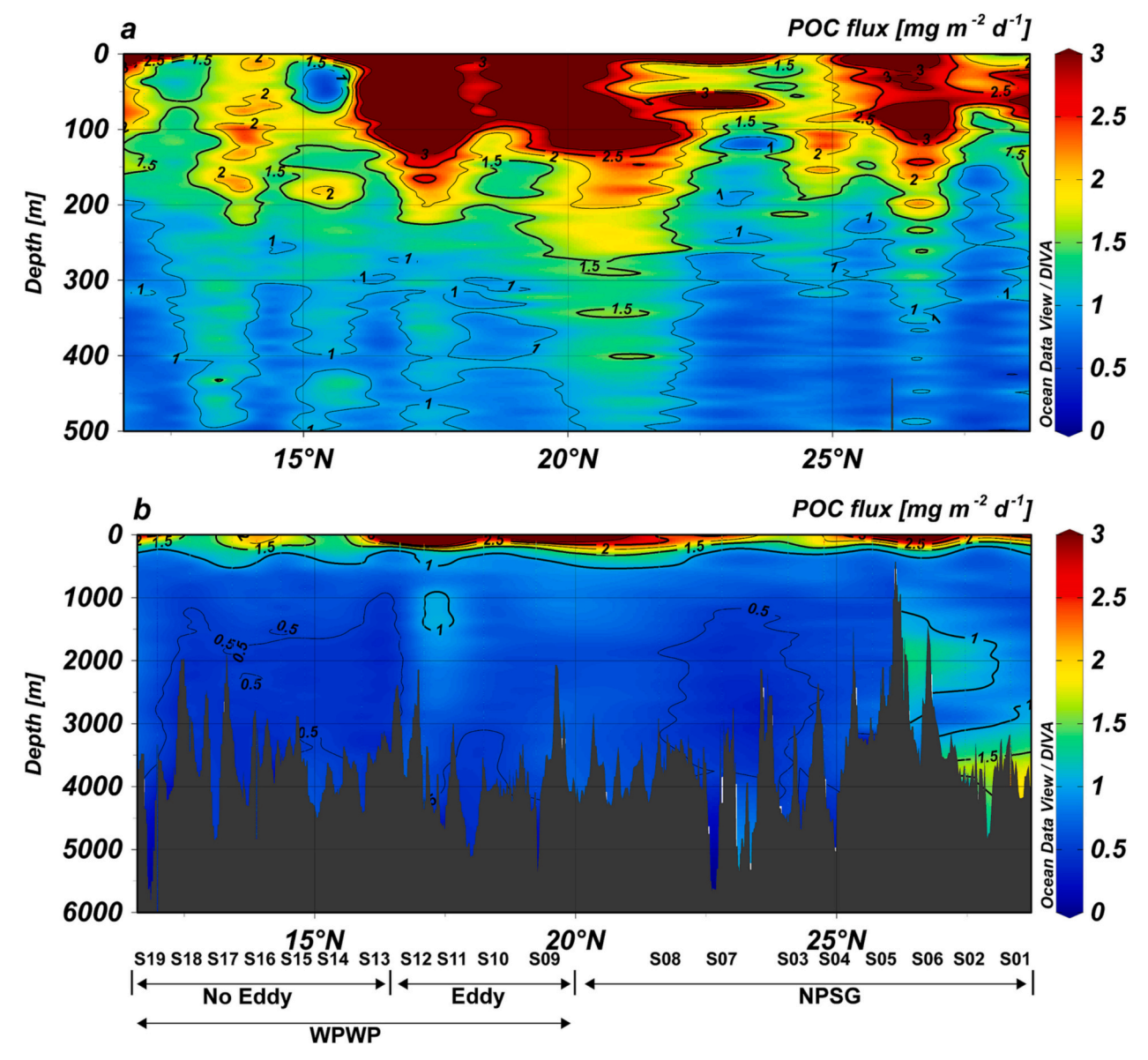


Fig. 4. Vertical distribution of POC flux along the south-north transect along the KPR. (a) 0-500 m; and (b) 0-6500 m.

contrast, while the POC flux associated with the medium and large particles also decreased with increasing depth, their relative contribution increased. A significant shift occurred in the near-bottom layer, in which both the POC flux associated with the small particles and their relative contribution were distinctly higher than those in the 3000 m layer (Figs. 5a, 6a). The above trends were present in both the NPSG and warm pool regions (Figs. 5b, c and 6b, c), but the magnitude of the variation was greater in the warm pool region than in the NPSG region (Figs. 7b, c).

In the NPSG, the near-bottom POC flux $(0.75\pm0.57~mg~m^{-2}~d^{-1})$ was higher than that in the 3000 m layer $(0.67\pm0.34~mg~m^{-2}~d^{-1})$, while the trend was reversed in the WPWP (near-bottom: $0.40\pm0.09~mg~m^{-2}~d^{-1}$; 3000 m: $0.48\pm0.09~mg~m^{-2}~d^{-1}$). This difference was also reflected in the vertical variation in the size structure of the particles. In the NPSG, the proportion of small particles increased from 44.2 % at 3000 m to 58.3 % in the near-bottom layer, while the proportions of the medium and large particles decreased from 41.7 % (3000 m) to 29.5 % (near-bottom) and from 14.1 % (3000 m) to 12.2 % (near-bottom), respectively. In the WPWP, the proportion of the small particles increased from 39.5 % at 3000 m to 55.8 % in the near-bottom layer, while the proportions of the medium and large particles decreased from

49.4 % (3000 m) to 36.9 % (near-bottom) and from 11.1 % (3000 m) to 7.3 % (near-bottom), respectively. The results of the PERMANOVA analysis revealed that the difference in the particle size structure between the 3000 m layer and the near-bottom layer was not significant ($R^2 = 0.197$, P = 0.054) in the NPSG, whereas the difference was significant ($R^2 = 0.331$, P = 0.002) in the WPWP.

3.3. Environmental factors and their influences on the POC flux

3.3.1. Chlorophyll

The chlorophyll-a concentration was low, and high chlorophyll-a concentrations occurred in the subsurface layer at depths of 50–150 m. Along the transect, the highest chlorophyll-a concentration (> 0.5 μg m $^{-2})$ occurred near 21°N (Fig. 8). The chlorophyll maximum layer was greater at a depth of 122 \pm 11 m south of 20°N than at a depth of 98 \pm 14 m north of 20°N.

Although there was a negative correlation between the integrated chlorophyll values and latitude, it was not statistically significant (P > 0.05; Fig. 9a). The relationship between the integrated chlorophyll values and the depth-specific POC flux is shown in Fig. 9b. The correlations were significant at depths of 200 m and 500 m (P = 0.018, P = 0.018).

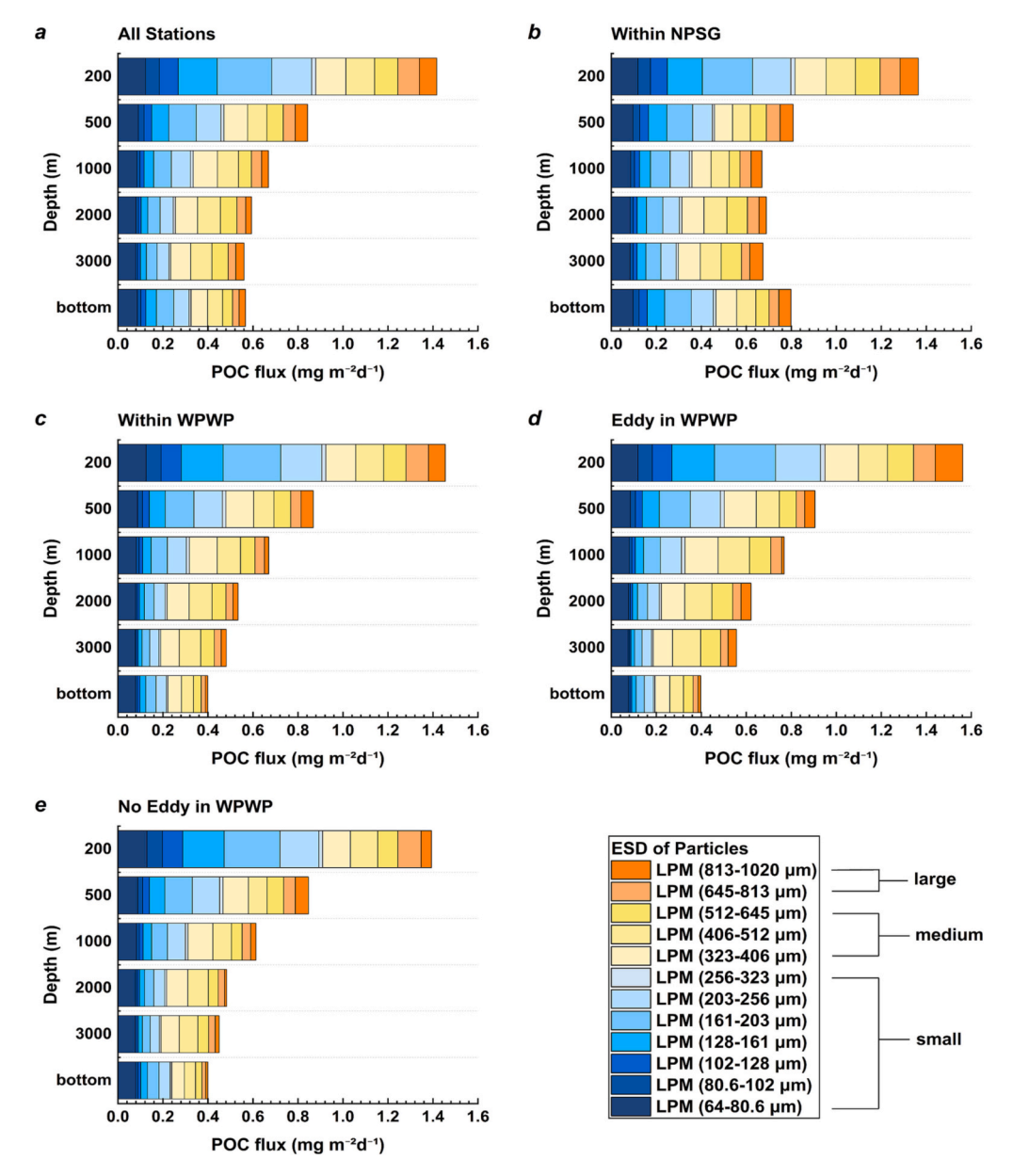


Fig. 5. Particle size structure and the size-specific contributions to the POC flux. (a) The total transect; (b) the sub-transect within the NPSG; (c) the sub-transect within the WPWP; (d) the sub-transect within the zone unaffected by eddies in the WPWP.

0.041, respectively) and were not significant at deeper depths.

3.3.2. Anticyclonic eddy

Positive SSHA values, indicating anticyclonic eddies (warm eddies), existed between 20 and $25^{\circ}N$ and $15-20^{\circ}N$ during this investigation. The SSHA values in the core of the warm eddies were 40 cm in the north and 20 cm in the south. However, based on the timing of the sampling at specific stations and the positions of the stations relative to the eddies, it was confirmed that the northern warm eddy had passed by the time of the survey and that the survey stations were located on the outside of the edge of the eddy (Figs. 10a, b), and hence, the northern warm eddy had no actual influence on the survey transect. In contrast, the southern warm eddy affected the survey transect (Figs. 10c, d).

3.3.3. Topography and current velocity

The survey transect was along the KPR. The KPR ranges from a minimum depth of <500 m to a maximum depth of over 6000 m, with slopes generally exceeding 10° and up to nearly 60° (Fig. 11). The

northern part of the KPR is more topographically more diverse than the southern part, with more seamounts with water depths of <1000 m. There are eight seamounts with depths of <1000 m north of $20^{\circ} N$, including seven north of $25^{\circ} N$. On the KPR south of $20^{\circ} N$, there are only two seamounts with depths of $\leq\!1000$ m (Fig. 11).

The current velocities along the entire transect in the 200 m, 500 m, 1000 m, and 1500 m water layers were 16.7 \pm 7.7 cm/s, 8.7 \pm 6.0 cm/s, 4.6 \pm 2.6 cm/s, and 4.0 \pm 2.1 cm/s, respectively. Compared to this, the current velocities north of 25°N along the transect in the 200 m, 500 m, 1000 m, and 1500 m layers were 29.3 \pm 7.0 cm/s, 18.6 \pm 5.5 cm/s, 8.4 \pm 2.5 cm/s, and 6.5 \pm 2.9 cm/s, respectively, which were 76, 113, 83, and 62 % higher than the mean values for entire transect (Fig. 12).

3.3.4. Influencing factors on the POC flux

The results of the multiple linear regression analysis are shown in Fig. 13. For the shallower depth range (< 1000 m), the POC fluxes in each layer were significantly positively correlated with the integrated chlorophyll concentration but were not correlated with the other

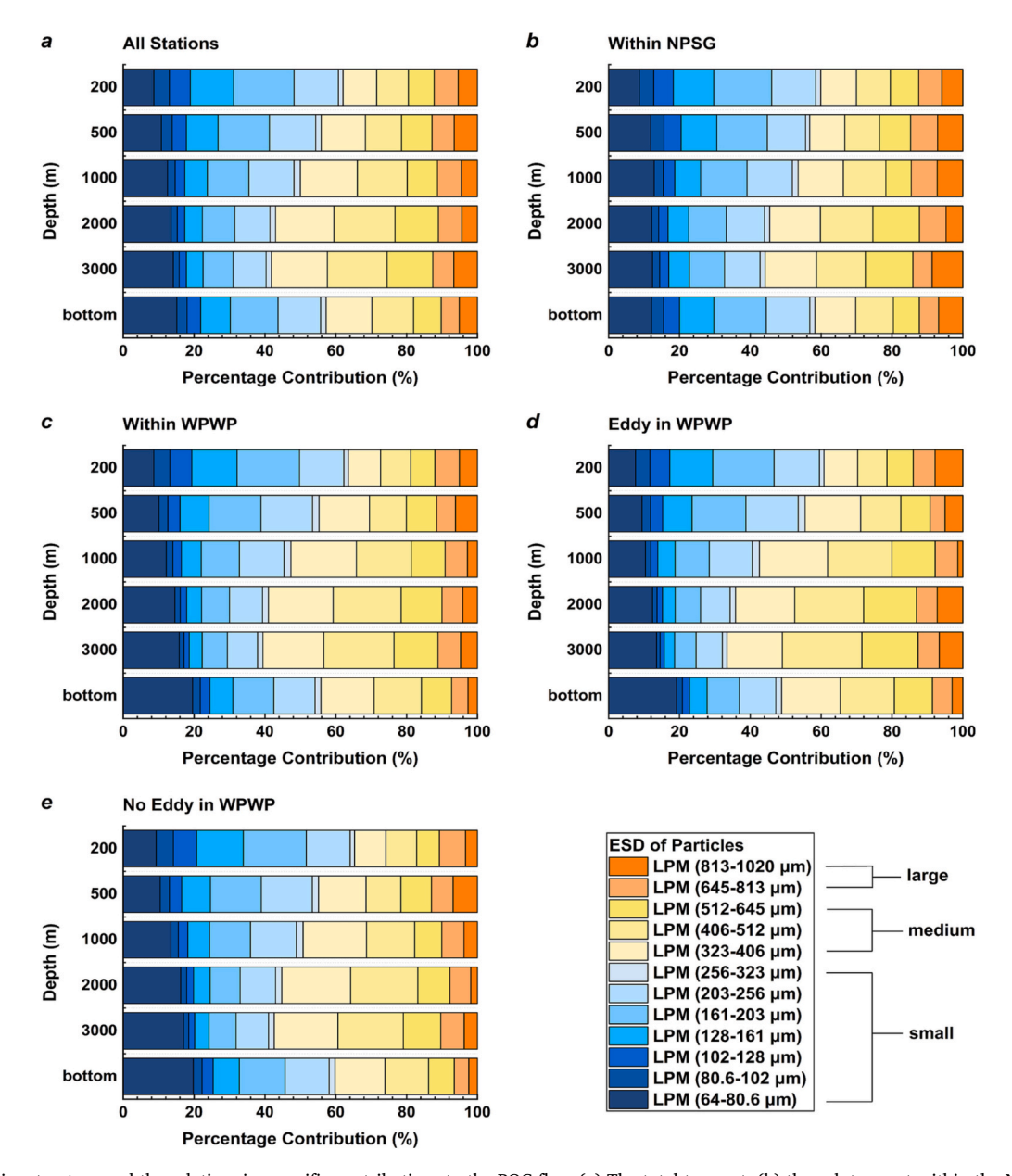


Fig. 6. Particle size structure and the relative size-specific contributions to the POC flux. (a) The total transect; (b) the sub-transect within the NPSG; (c) the sub-transect within the WPWP; (d) the sub-transect within the mesoscale eddy-influenced zone in the WPWP; and (e) the sub-transect within the zone unaffected by eddies in the WPWP.

factors. For the depth range of 1000 m to 3000 m, the POC fluxes in each layer were significantly positively correlated with the integrated chlorophyll concentration, sea surface height anomaly (SSHA), and T-V. For the near-bottom layers, the POC fluxes were only significantly positively correlated with the SSHA and T-V (Fig. 13).

4. Discussion

4.1. Effect of anticyclonic eddy on POC fluxes at the KPR

Global observations have shown that the western Pacific has a high abundance of mesoscale eddies (Chelton et al., 2007). The eddy kinetic energy, which is used to characterize the intensity of the eddy activity, has a significant high value zone in the tropical-subtropical western Pacific (Ji et al., 2020). Mesoscale eddies can influence the distribution of particles and regulate about one third of the carbon flux in the oceans (Waite et al., 2016). The mechanisms by which cyclonic and

anticyclonic eddies cause increases in the POC fluxes are different. The magnitude of the output fluxes in the ocean is generally dependent on the nutrient inputs to the euphotic zone (EZ), and the mechanism by which cyclonic eddies increase the output is mainly by increasing nutrient inputs to the EZ and enhancing the primary productivity, which in turn cause increases in the POC fluxes that are mainly confined to the upper ocean. In 38 cyclonic eddies observed between 1993 and 2018, the POC, PON, and biogenic Si fluxes were found to be spatially enhanced in the core and margins of the eddy, with the highest POC, PON, and biogenic Si fluxes occurring transiently during the eddy maturation phase (3-8 weeks) (Zhou et al., 2021). However, from the western marginal sea to the oligotrophic open ocean, the influence of the cold eddies on the upper ocean decreases (from 91 \pm 12 % to 6 \pm 5 % for nutrients and from 12 \pm 5 % to 2 \pm 1 % for the chlorophyll concentrations) (Huang and Xu, 2018). The impact of cyclonic eddies is even higher in the eastern marginal seas than in the oligotrophic open ocean, which is probably due to the presence of coastal upwelling, as reported

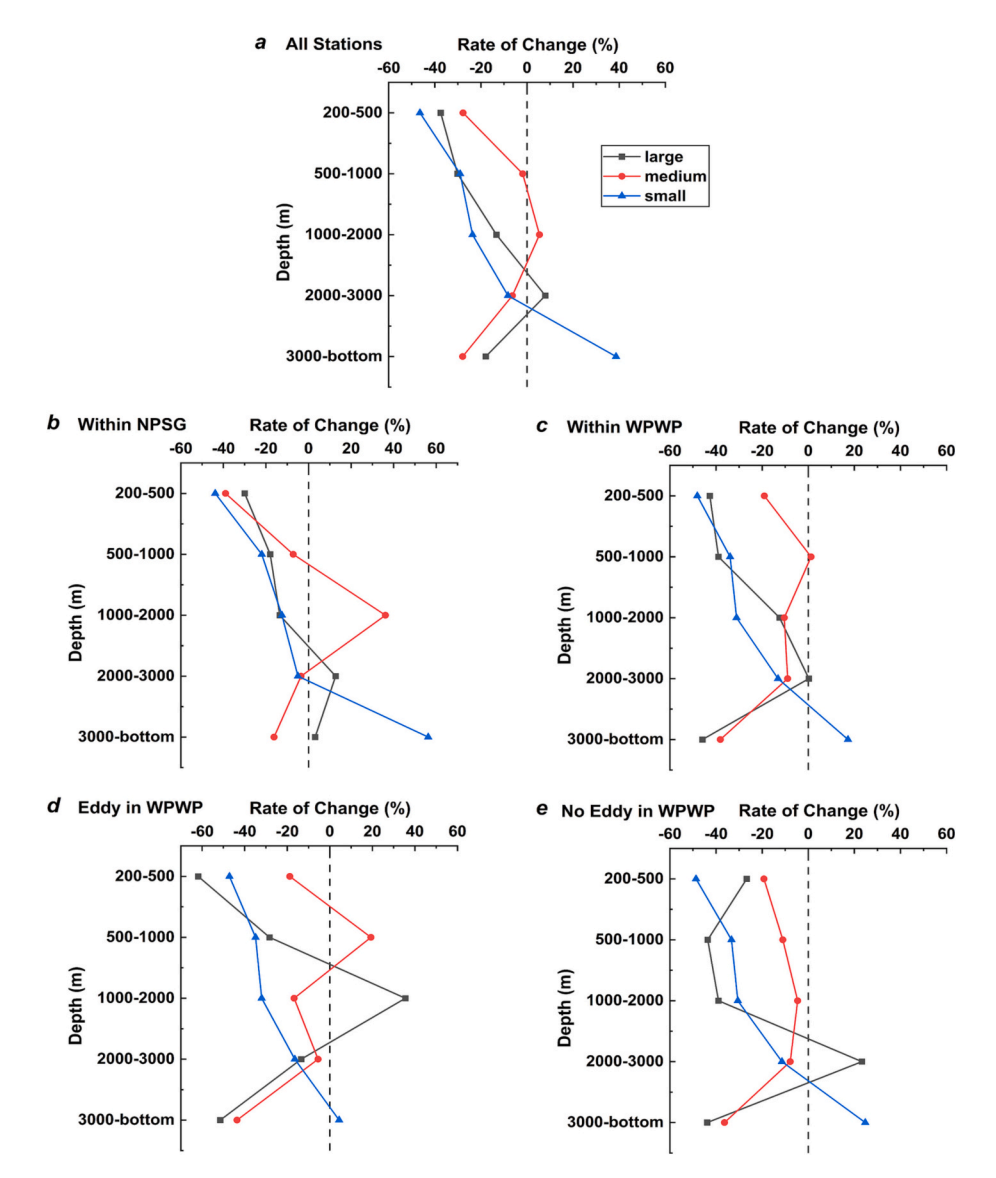


Fig. 7. The rates of change of the three sizes of particles between the layers. (a) The total transect; (b) the sub-transect within the NPSG; (c) the sub-transect within the WPWP; (d) the sub-transect within the zone influenced by mesoscale eddies in the WPWP; and (e) the sub-transect within the zone unaffected by eddies in the WPWP.

by Amos et al. (2019) for the enhancement of POC fluxes in the Californian upwelling region by cyclonic eddies. In contrast to cyclonic eddies, anticyclonic eddies with downwelling in the core region are not conducive to nutrient flux into the true photosphere and thus may inhibit particle export. However, a study conducted in the northern oligotrophic basin of the South China Sea found that the presence of anticyclonic eddies led to an increase in particle export flux due to the presence of anticyclonic eddies (Zhou et al., 2013). The phenomenon of higher chlorophyll concentrations at the edges of anticyclonic eddies and a higher POC output at the center observed in the northern South China Sea may be the result of a combination of vertical convection and lateral transport within the eddies (Wang et al., 2018). One explanation is that the center of the anticyclonic eddy is irradiated and sinking, and due to some dynamic mechanisms, the downward output of the POC flux can be achieved and can reach the deeper ocean. For example, Waite et al. (2016) found that the particles in the eddy funnel into a wineglassshaped distribution at a depth of 1000 m, resulting in a sevenfold increase in the vertical carbon flux in the center of the eddy relative to the sides of the eddy, i.e., the wineglass effect, while smaller, slower sinking particles spent more time in the center of the eddy. Another observation by Andres et al. (2019) in northern Palau in the western Pacific Ocean

confirmed the significant influence of mesoscale eddies on the deep-sea current, even at depths of >4200 m. In this study, the POC fluxes in the water column within the anticyclonic eddies were about 0.2 mg m $^{-2}$ d $^{-1}$ higher than at the other stations outside the eddy, except near the bottom. This means that the transit of the anticyclonic eddies causes an increase in the POC fluxes above the KPR. The wineglass effect described above may be the cause of this phenomenon. Considering that there are more anticyclonic eddies than cyclonic eddies in the tropical western Pacific (Hu et al., 2018) and the high occurrence of anticyclonic eddies in this region, anticyclonic eddies have a non-negligible influence when quantifying the POC fluxes in the tropical western Pacific.

4.2. Impact of topography

As the currents flow over the seamounts, they interact with the steep and complex topography and generate a variety of physical processes (Dai et al., 2022). In many practical observations, an increase in sediment fluxes has been observed in the deep and near-bottom layers in the vicinity of seamounts or on land slopes (Ma et al., 2019). Misic et al. (2012) conducted a study on the shallow Tyrrhenian seamounts and found that organic matter fluxes were observed downstream of the

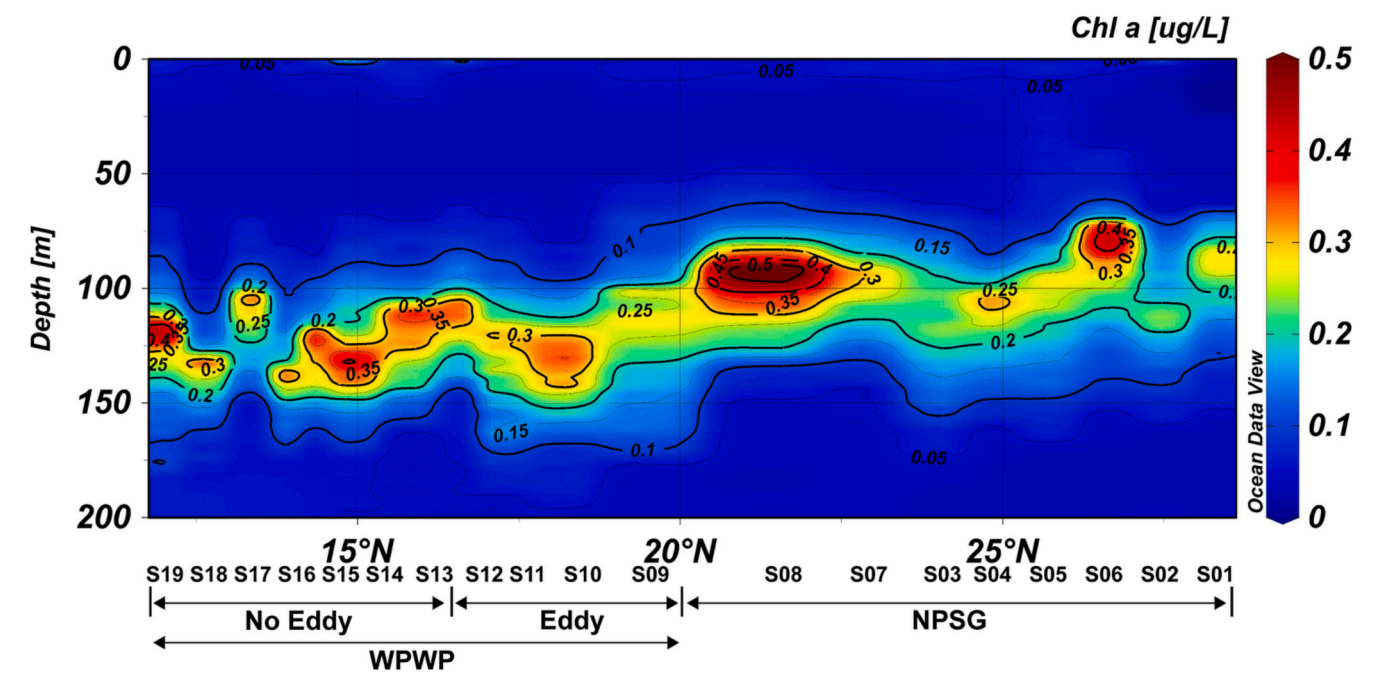


Fig. 8. Vertical distribution of chlorophyll-a concentration along the south-north transect along the KPR.

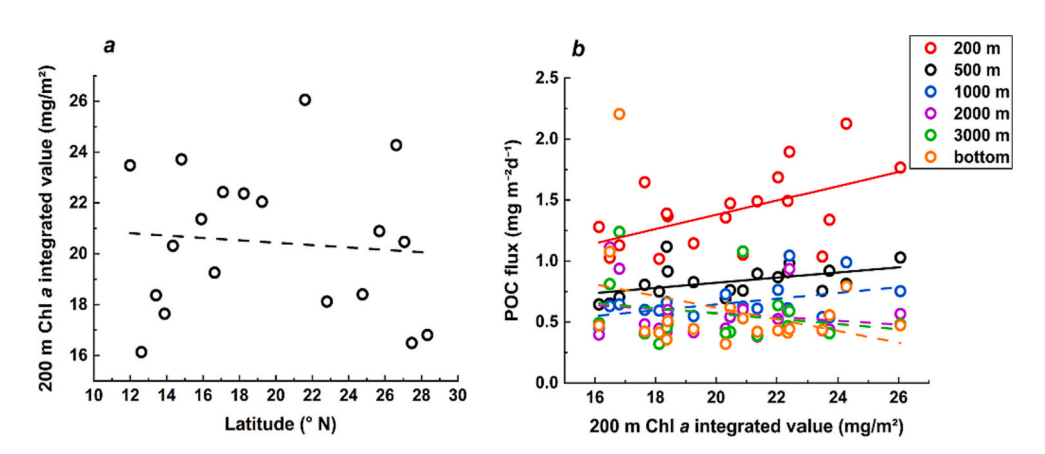


Fig. 9. (a) Relationship between the integrated chlorophyll values and latitude along the transect; and (b) Relationship between the integrated chlorophyll values and the depth-specific POC flux along the transect. The statistically significant correlations are shown as solid lines, and the non-significant correlations are shown as dashed lines.

seamounts, at the bottom and further down the flanks of the seamounts, and in the deeper (mesopelagic) layers; further, increased OM due to sediment deposition and resuspension of sediments along the land slope/flank was recorded. A study of the Senghor Seamount in the tropical Atlantic similarly found that the effects of the topographiccurrent interactions at seamounts exported POC from the surface (up to 6100 m) into the deeper ocean. The POC output at seamount sites was 2-4 times higher than at reference sites and the highest fluxes on the downstream side of the seamount (Turnewitsch et al., 2016). In the tropical subtropical western Pacific, there are a variety of large-scale circulation currents that extend to the KPR seamount chain and may lead to a more complex flow field structure that affects the hydrodynamic environment of the ocean and has implications for the POC fluxes in the deeper layers. In the northern part of the study area, increased POC fluxes were also observed in the deep and near-bottom layers. Regarding this increase in POC fluxes on the seamounts, a recent modeling approach based on sensitivity experiments revealed that the presence of seamounts leads to a more complex flow field structure around them, increasing local flow velocities and promoting fronts and rapids in the boundary layer at the base of the seamount, thus causing an increase in the resuspension intensity in the near-bottom layer of the seamount (Jiang et al., 2021). In addition, lateral transport is a factor that cannot be ignored, and organic matter resuspended from the sediment surface may be laterally transported from the local area or the land slope to the deep sea by certain currents (Druffel et al., 1998). Studies using sediment traps in the South China Sea have provided good evidence. For example, Gao et al. (2020) studied particles collected using sediment traps in the northern South China Sea and found that they were mainly derived from lateral transport along the land slope. Ran and Chen (2022) conducted a study in the northwestern South China Sea and also found that laterally transported resuspended sediments accounted for a large proportion of the deep-sea particle flux. Hwang et al. (2009) moored time-series sediment traps on the New England slope and found that the fluxes of sinking POC were frequently higher and the ¹⁴C values of the sinking POC were low at deeper depths compared to the shallower sediments, providing strong evidence for the lateral transport of older organic matter at the margin, with the resuspended sediments transported by the currents forming the so-called nepheloid layers. In our

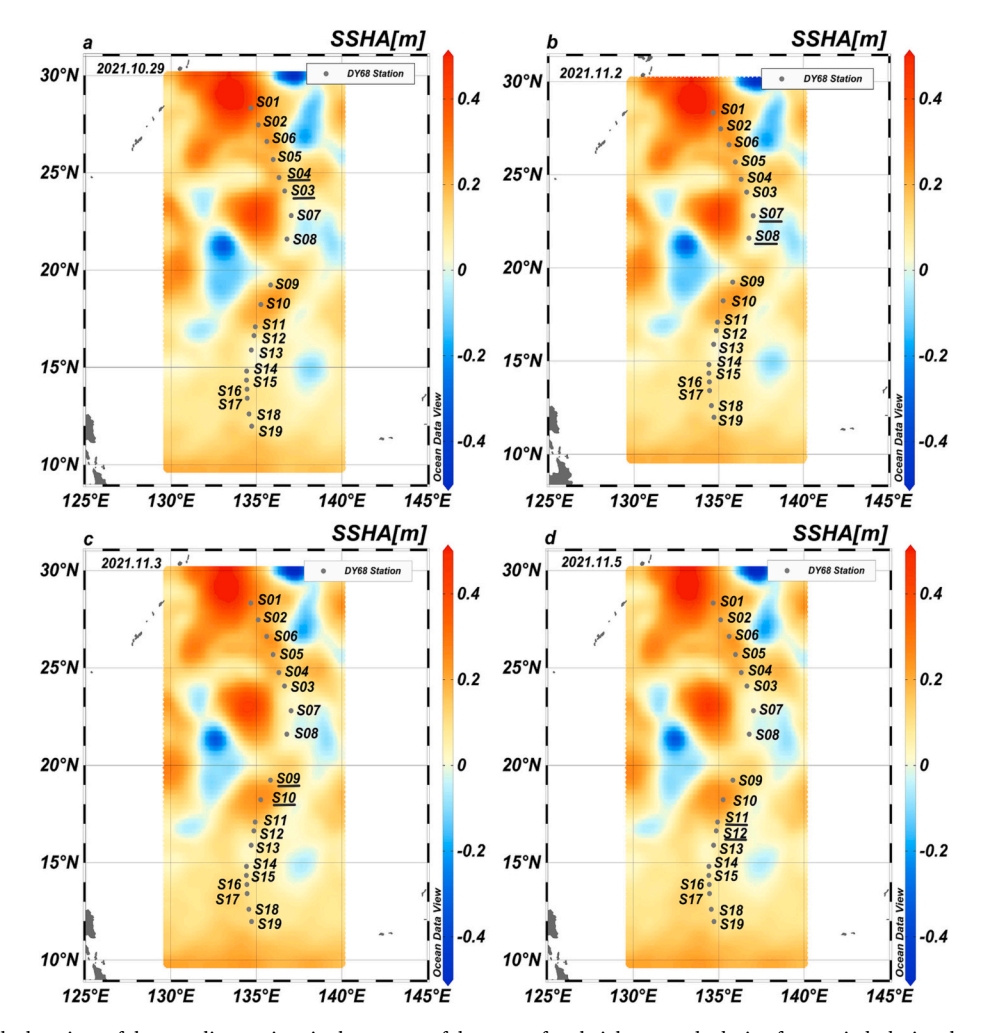


Fig. 10. Map showing the locations of the sampling stations in the context of the sea surface height anomaly during four periods during the cruise. The station names underlined in black are the survey stations measured on that day.

study area, most of the seamounts shallower than 1000 m are distributed north of 25°N, and high current velocities also occur in the north. Based on the results of the multiple linear regressions, the effect of the interaction between the topography and current velocity is significant at depths of $\geq\!2000$ m. According to the above evidence, it can be hypothesized that the interaction of the complex topography and higher current velocity leads to resuspension and lateral migration of sediments, thus causing an increased flux in the deeper layers in the north. The topography and current velocity are constant factors on longer time scales, and therefore, the increased flux caused by these factors must be particularly noted, and shallow seamount areas with similar topography are potential areas of sustained high POC fluxes.

4.3. Composition of particulate matter, decay processes, the important role of tiny particles

Buesseler et al. (2007b) conducted a comparison study at station K2 in the North Pacific Ocean and station ALOHA in the NPSG and found that the attenuation of the POC fluxes in the twilight zone was not determined by the magnitude of the flux but by the nature of the output POC (e.g., particle size and composition) and the site-specific mesopelagic processes. The relationship between the particle size and carbon export fluxes of particles settling in the ocean has long been a hot research topic. The traditional view is that larger particles, such as zooplankton feces, have high settling rates and that large particles are the major contributors to oceanic POC fluxes (Fowler and Knauer, 1986). However, recent studies have shown that slowly settling small

particles (< 100 μm) also play an important role in oceanic carbon fluxes, and that they typically experience relatively little decay with increasing depth, particularly in oligotrophic low flux oceanic environments where small particles can contribute up to 46 % of the deepsea carbon flux (Durkin et al., 2021). The results of Cael et al. (2021) also highlight the importance of not only the size but also the composition, structure, and/or density in determining particle sinking rates, for example, small aggregates can sink at rates similar to those of large aggregates. Our results also confirm the important contribution of small particles to the POC flux, with the fraction of small particles consistently ranging between 40 and 60 % in all of the water layers, and the positive contribution of small particles to near-bottom POC flux enhancement.

4.4. Spatial variation in deep-sea POC flux along the KPR and implications for deep sea benthic ecosystems

Only a small fraction of the carbon fixed by primary production is exported from the upper ocean to the deep sea. At greater depths, respiration by marine organisms still consumes significant amounts of POC. For example, Koppelmann et al. (2004) observed that in the eastern Mediterranean, medium-sized zooplankton consumed 23 % of the sinking POC flux between 1050 m and 4250 m. Henson et al. (2012) studied global patterns of POC export to the deep ocean and found that only a small fraction (\sim 1–5 %) of the particulate organic matter from primary production at low latitudes was exported, most of which was remineralized in the upper ocean (< 100 m), while about 20–35 % of the final exported POC sank and was preserved at a depth of 2000 m,

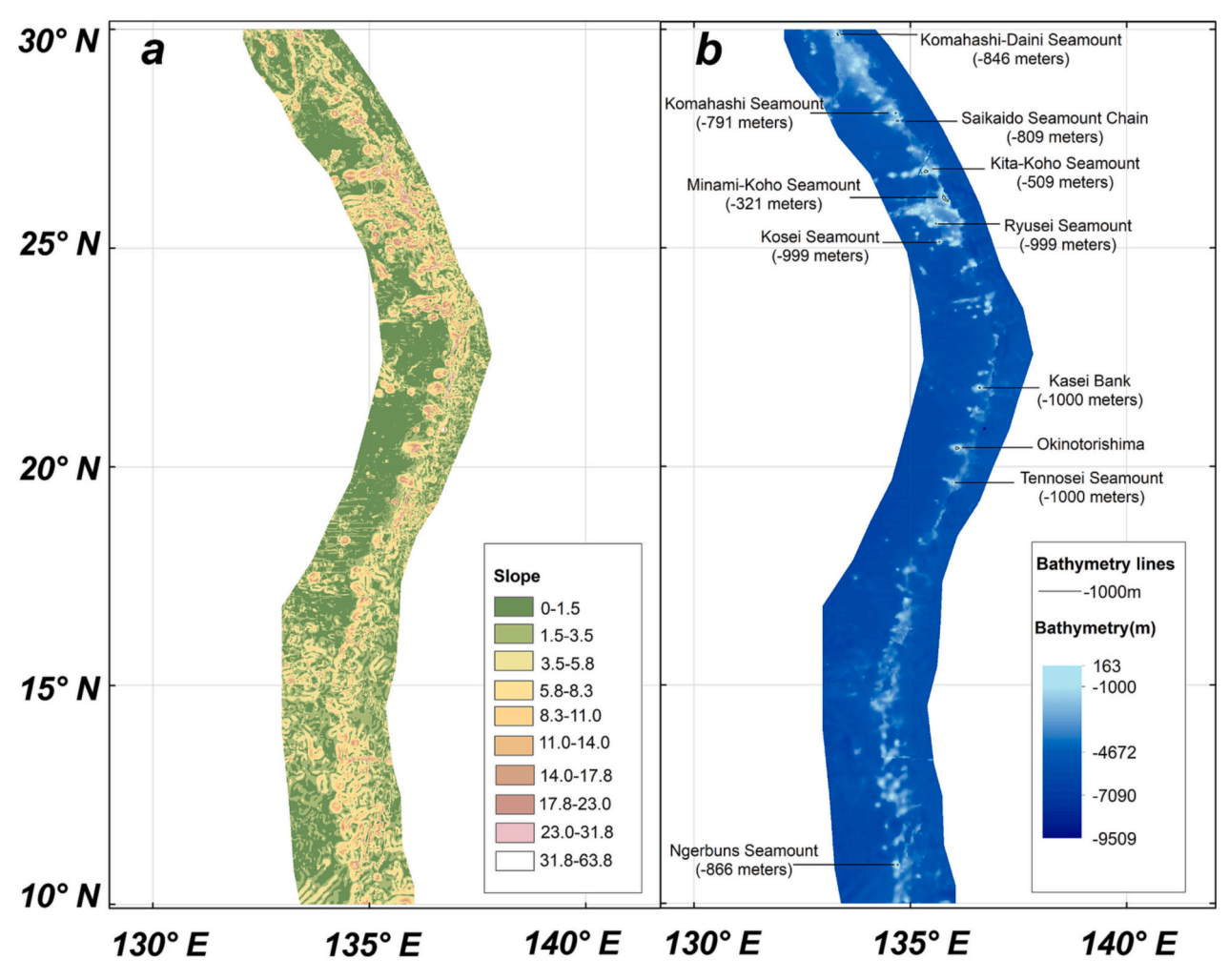


Fig. 11. (a) The slope of the KPR and (b) the bathymetry of the KPR showing the seamounts at depths of <1000 m.

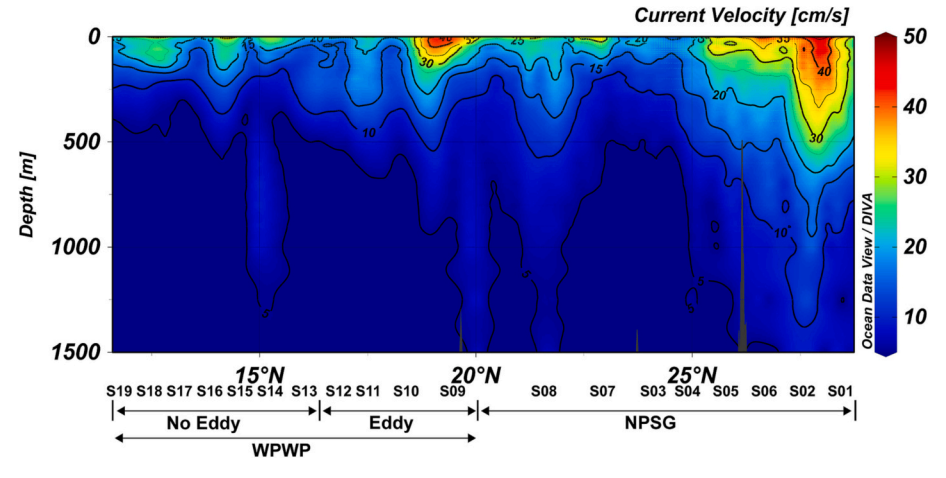


Fig. 12. Vertical distribution of the current velocity along the south-north transect along the KPR.

suggesting that the particulate matter exported from low latitudes is more insoluble and undergoes little further remineralization at mesopelagic depths. A similar pattern was found in this study, that is, 37 % of the POC output from a depth of 200 m was preserved to 2000 m in the WPWP, and up to 51 % was preserved in the NPSG, suggesting that the NPSG region has a higher efficiency of POC output to the deep sea than the WPWP region.

The final fate of particulate matter that sinks into the deep sea is either ingestion as food for benthic organisms and demersal fish or deposition on the seafloor for temporary deposition until the next resuspension. The benthic communities on seamounts are dominated by filter feeders that rely on this sunken POC as a food source, such as the cold-water coral reefs that live in the deep sea and feed on these particles (Duineveld et al., 2004; Maier et al., 2023). It is clear that the quantity

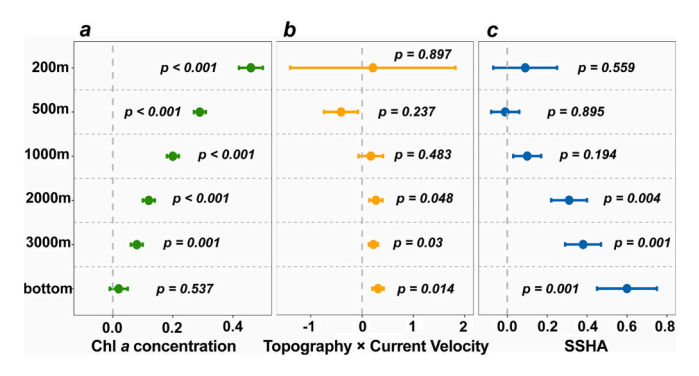


Fig. 13. Results of multiple linear regression of the POC flux and three environmental factors in each depth layer showing the coefficients of the regression and significance. (a) integrated chlorophyll concentration; (b) interaction effect between the topography and current velocity (T-V); and (c) Sea surface height anomaly (SSHA).

and quality of POC fluxes are important ecological drivers in the deep sea, and that deep-sea ecosystems are highly sensitive to changes in POC fluxes (Tittensor et al., 2011). The results of our study also highlight the distribution of POC fluxes in different regions of the deep sea. On a latitudinal gradient, the POC fluxes are higher in the northern part of the study area, where chlorophyll levels are high and there is an interaction between shallow water seamounts and the flow field, than in the southern part of the study area. Along the depth gradient, the POC fluxes initially attenuate and then increase to varying degrees near the bottom due to resuspension at seamounts, resulting in additional POC supply. In addition, the transit of mesoscale eddies also results in a short-term high POC supply to benthic communities at depths of 3000 m.

Many observations suggest that climate change is already affecting the deep-sea environment today, leading to increased deep-sea temperatures and altered POC fluxes to the seafloor (Ruhl and Smith, 2004; Smith et al., 2013). Recent studies have recorded a decrease in POC fluxes to the seafloor in most tropical and subtropical ocean regions; while in some high latitude oceans, POC fluxes have increased (Jones et al., 2014; Sweetman et al., 2017). The KPR is located in the tropics and subtropics and therefore faces an overall trend of decreasing POC fluxes in the context of global warming. The northern part of the KPR is located in the NPSG, which has a clear trend of increasing SST and stratification due to global warming on interannual and decadal time scales (Dai et al., 2023). Factors that can lead to increased local POC fluxes, such as shallow-water seamounts and a high incidence of mesoscale eddies, are of greater ecological importance when benthic organisms are faced with more stressful environments with food scarcity.

4.5. Methodological limitations

Compared to the widely used sediment trap-based methods for estimating POM/POC fluxes in the ocean, the method used in this study has some limitations, mainly in the following aspects. First, in contrast to sediment trap data, data obtained from UVP measurements are transient (Picheral et al., 2022) and therefore do not capture temporal scale variations (especially seasonal changes). Second, a UVP measures the particle size and number data of particulate matter, which does not allow direct measurement of the POM/POC mass and requires indirect calculations based on empirical formulas (Giering et al., 2020; Guidi et al., 2008). Third, even with the latest version of UVP equipment (UVP 6.0), the effective resolution can only capture particles larger than 60 μm , thus making it impossible to assess the contribution of particulate matter smaller than this size to the total flux. Fortunately, particulate matter of this size typically accounts for a small fraction of the total flux (Durkin et al., 2021) and sinks extremely slowly (Cael et al., 2021). Thus, this issue had little impact on our study of the POC fluxes into the deep ocean. Despite the methodological limitations mentioned above, in this study, the distribution of particulate matter in the ocean was measured using a UVP, and the POC fluxes were estimated based on the particle size-sedimentation equation of particulate matter in the ocean. We obtained results comparable to those attained using traditional sediment trap methods. Therefore, this POC flux measurement method, which can provide much higher horizontal and vertical resolutions than traditional methods, can be applied more in the future to provide high-resolution material flux data for deep-sea ecosystem studies.

5. Conclusions

Along a latitudinal gradient along the KPR, 37 % of the POC output from a depth of 200 m was preserved to 2000 m in the WPWP, and up to 51 % was presented in the NPSG, suggesting that the NPSG region has a higher efficiency of POC output to the deep sea than the WPWP region. The variation in the POC fluxes with depth was size-specific, with small particles decaying in the mesopelagic and deep layers and increasing in the near-bottom layer, while an increase in large particles occurred in the 2000-3000 m layer in anticyclonic eddies. The chlorophyll concentration of the upper ocean had a significant positive effect on the POC fluxes at all depths, except near the bottom, while local factors such as mesoscale eddies and the interaction effect between the topography and current velocity only had significant effects on the POC fluxes at depths deeper than 2000 m. The increase in the POC fluxes due to an anticyclonic eddy was temporary, while the increase in the POC fluxes due to topography-current velocity interactions was persistent. The results of this study provided key fundamental data for the cartography of the distribution and simulation of the dynamics of deep-sea organisms along the KPR in the Philippine Sea.

CRediT authorship contribution statement

Ziyu Wang: Methodology, Data curation, Formal analysis, Writing – original draft. **Chen Fang:** Investigation. **Chenghao Yang:** Data curation, Formal analysis. **Guoyin Zhang:** Data curation, Formal analysis. **Dong Sun:** Conceptualization, Data curation, Writing – review & editing, Supervision, Funding acquisition.

Declaration of competing interest

The authors declare that they have no known competing financial interests or personal relationships that could have appeared to influence the work reported in this paper.

Data availability

Data will be made available on request.

Acknowledgments

This work was supported by the National Natural Science Foundation of China (grant number: 42076122), the Project of State Key Laboratory of Satellite Ocean Environment Dynamics, Second Institute of Oceanography (SOEDZZ2201), and the China Ocean Mineral Resources Research and Development Association Program (grant numbers: DY-XZ-02). We thank Mr. Linjie Zhang for his assistance in statistical method. We thank the captain and crew of the R/V SHENHAIYIHAO for their assistance with sampling. We thank LetPub (www.letpub.com) for its linguistic assistance during the preparation of this manuscript.

References

Alldredge, A.L., Silver, M.W., 1988. Characteristics, dynamics and significance of marine snow. Prog. Oceanogr. 20, 41–82. https://doi.org/10.1016/0079-6611(88)90053-5. Allison, D.B., Stramski, D., Mitchell, B.G., 2010. Seasonal and interannual variability of particulate organic carbon within the Southern Ocean from satellite ocean color

- observations. J. Geophys. Res. 115, C06002. https://doi.org/10.1029/
- Al-Mutairi, H., Landry, M.R., 2001. Active export of carbon and nitrogen at Station ALOHA by diel migrant zooplankton. Deep Sea Res. Part II Top. Stud. Oceanogr. 48, 2083–2103. https://doi.org/10.1016/S0967-0645(00)00174-0.
- Amos, C.M., Castelao, R.M., Medeiros, P.M., 2019. Offshore transport of particulate organic carbon in the California Current System by mesoscale eddies. Nat. Commun. 10, 4940. https://doi.org/10.1038/s41467-019-12783-5.
- Andres, M., Siegelman, M., Hormann, V., Musgrave, R.C., Merrifield, S.T., Rudnick, D.L., Merrifield, M.A., Alford, M.H., Voet, G., Wijesekera, H.W., MacKinnon, J.A., Centurioni, L., Nash, J.D., Terrill, E.J., 2019. Eddies, topography, and the abyssal flow by the Kyushu-Palau Ridge near Velasco Reef. Oceanography 32 (4), 46–55. https://doi.org/10.5670/oceanog.2019.410.
- Arístegui, J., Duarte, C.M., Agustí, S., Doval, M., Álvarez-Salgado, X.A., Hansell, D.A., 2002. Dissolved organic carbon support of respiration in the dark ocean. Science 298, 1967.
- Baltar, F., Arístegui, J., Gasol, J.M., Sintes, E., Herndl, G.J., 2009. Evidence of prokaryotic metabolism on suspended particulate organic matter in the dark waters of the subtropical North Atlantic. Limnol. Oceanogr. 54, 182–193. https://doi.org/ 10.4319/lo.2009.54.1.0182.
- Bisson, K., Siegel, D.A., DeVries, T., 2020. Diagnosing mechanisms of ocean carbon export in a satellite-based food web model. Front. Mar. Sci. 7, 505. https://doi.org/ 10.3389/fmars.2020.00505.
- Bleck, R., 2002. An oceanic general circulation model framed in hybrid isopycnic-Cartesian coordinates. Ocean Model 4, 55–88. https://doi.org/10.1016/S1463-5003
- Buesseler, K.O., Antia, A.N., Chen, M., Fowler, S.W., Gardner, W.D., Gustafsson, O., Harada, K., Michaels, A.F., Rutgers van der Loeff, M., Sarin, M., Steinberg, D.K., Trull, T., 2007a. An assessment of the use of sediment traps for estimating upper ocean particle fluxes. J. Mar. Res. 65, 345–416. https://doi.org/10.1357/002224007781567621.
- Buesseler, K.O., Lamborg, C.H., Boyd, P.W., Lam, P.J., Trull, T.W., Bidigare, R.R., Bishop, J.K.B., Casciotti, K.L., Dehairs, F., Elskens, M., Honda, M., Karl, D.M., Siegel, D.A., Silver, M.W., Steinberg, D.K., Valdes, J., Van Mooy, B., Wilson, S., 2007b. Revisiting carbon flux through the ocean's twilight zone. Science 316, 567–570. https://doi.org/10.1126/science.1137959.
- Cael, B.B., Cavan, E.L., Britten, G.L., 2021. Reconciling the size-dependence of marine particle sinking speed. Geophys. Res. Lett. 48 https://doi.org/10.1029/ 2020GL091771.
- CBD, 2016. Report of the Regional Workshop to Facilitate the Description of Ecologically or Biologically Significant Marine Areas in the Seas of East Asia (No. UNEP/CBD/SBSTTA/20/INF/24). UNEP, Montreal, Canada.
- Chelton, D.B., Schlax, M.G., Samelson, R.M., de Szoeke, R.A., 2007. Global observations of large oceanic eddies: GLOBAL OBSERVATIONS OF OCEANIC EDDIES. Geophys. Res. Lett. 34 https://doi.org/10.1029/2007GL030812.
- Dai, S., Zhao, Y., Li, X., Wang, Z., Zhu, M., Liang, J., Liu, H., Sun, X., 2022. Seamount effect on phytoplankton biomass and community above a deep seamount in the tropical western Pacific. Mar. Pollut. Bull. 175, 113354 https://doi.org/10.1016/j.marpolbul.2022.113354.
- Dai, M., Luo, Y., Achterberg, E.P., Browning, T.J., Cai, Y., Cao, Z., Chai, F., Chen, B., Church, M.J., Ci, D., Du, C., Gao, K., Guo, X., Hu, Z., Kao, S., Laws, E.A., Lee, Z., Lin, H., Liu, Q., Liu, X., Luo, W., Meng, F., Shang, S., Shi, D., Saito, H., Song, L., Wan, X.S., Wang, Y., Wang, W., Wen, Z., Xiu, P., Zhang, J., Zhang, R., Zhou, K., 2023. Upper ocean biogeochemistry of the oligotrophic North Pacific subtropical gyre: from nutrient sources to carbon export. Rev. Geophys. https://doi.org/10.1029/2022RG000800
- Ding, H., Ding, W., Zhao, Y., Riel, B., 2022. Spatiotemporal distribution of seamount volume along the Kyushu-Palau Ridge: implications for rejuvenated volcanism. J. Asian Earth Sci. 240, 105391 https://doi.org/10.1016/j.jseaes.2022.105391.
- Druffel, E.R.M., Griffin, S., Bauer, J.E., Wolgast, D.M., Wang, X.-C., 1998. Distribution of particulate organic carbon and radiocarbon in the water column from the upper slope to the abyssal NE Pacific Ocean. Deep Sea Res. Part II Top. Stud. Oceanogr. 45, 667–687. https://doi.org/10.1016/S0967-0645(98)00002-2.
- Duineveld, G., Lavaleye, M., Berghuis, E., 2004. Particle flux and food supply to a seamount cold-water coral community (Galicia Bank, NW Spain). Mar. Ecol. Prog. Ser. 277, 13–23. https://doi.org/10.3354/meps277013.
- Durkin, C.A., Buesseler, K.O., Cetinić, I., Estapa, M.L., Kelly, R.P., Omand, M., 2021. A visual tour of carbon export by sinking particles. Glob. Biogeochem. Cycles 35. https://doi.org/10.1029/2021GB006985.
- Fowler, S.W., Knauer, G.A., 1986. Role of large particles in the transport of elements and organic compounds through the oceanic water column. Prog. Oceanogr. 16, 147–194. https://doi.org/10.1016/0079-6611(86)90032-7.
- Gao, M., Huang, B., Liu, Z., Zhao, Y., Zhang, Y., 2020. Observations of marine snow and fecal pellets in a sediment trap mooring in the northern South China Sea. Acta Oceanol. Sin. 39, 141–147. https://doi.org/10.1007/s13131-020-1561-9.
- Giering, S.L.C., Cavan, E.L., Basedow, S.L., Briggs, N., Burd, A.B., Darroch, L.J., Guidi, L., Irisson, J.-O., Iversen, M.H., Kiko, R., Lindsay, D., Marcolin, C.R., McDonnell, A.M. P., Möller, K.O., Passow, U., Thomalla, S., Trull, T.W., Waite, A.M., 2020. Sinking organic particles in the ocean—flux estimates from in situ optical devices. Front. Mar. Sci. 6, 834. https://doi.org/10.3389/fmars.2019.00834.
- Gillard, B., Harbour, R.P., Nowald, N., Thomsen, L., Iversen, M.H., 2022. Vertical distribution of particulate matter in the Clarion Clipperton Zone (German Sector) potential impacts from deep-sea mining discharge in the water column. Front. Mar. Sci. 9, 820947 https://doi.org/10.3389/fmars.2022.820947.
- Girault, M., Gregori, G., Barani, A., Arakawa, H., 2016. A study of microphytoplankton and cyanobacteria consortia in four oligotrophic regimes in the western part of the

- North Pacific subtropical gyre and in the warm pool. J. Plankton Res. 38, 1317–1333. https://doi.org/10.1093/plankt/fbw056.
- Gooday, A.J., 2002. Biological responses to seasonally varying fluxes of organic matter to the ocean floor: a review. J. Oceanogr. 58, 305–332.
- Guidi, L., Jackson, G.A., Stemmann, L., Miquel, J.C., Picheral, M., Gorsky, G., 2008. Relationship between particle size distribution and flux in the mesopelagic zone. Deep-Sea Res. I: Oceanogr. Res. Pap. 55, 1364–1374. https://doi.org/10.1016/j. dsr. 2008.05.014.
- Guidi, L., Legendre, L., Reygondeau, G., Uitz, J., Stemmann, L., Henson, S.A., 2015.
 A new look at ocean carbon remineralization for estimating deepwater sequestration: ocean remineralization and sequestration. Glob. Biogeochem. Cycles 29, 1044–1059. https://doi.org/10.1002/2014GB005063.
- Halliwell, G., Bleck, R., Chassignet, E., 1998. Atlantic Ocean simulations performed using a new hybrid-coordinate ccean model. EOS Trans. AGU. Fall 1998 AGU meeting.
- Halliwell, G.R., Bleck, R., Chassignet, E.P., Smith, L.T., 2000. Mixed layer model validation in Atlantic Ocean simulations using the Hybrid Coordinate Ocean Model (HYCOM). EOS 80, OS304.
- Henson, S.A., Sanders, R., Madsen, E., 2012. Global patterns in efficiency of particulate organic carbon export and transfer to the deep ocean: export and transfer efficiency. Glob. Biogeochem. Cycles 26, n/a-n/a. https://doi.org/10.1029/2011GB004099.
- Honda, M.C., Kawakami, H., Matsumoto, K., Wakita, M., Fujiki, T., Mino, Y., Sukigara, C., Kobari, T., Uchimiya, M., Kaneko, R., Saino, T., 2016. Comparison of sinking particles in the upper 200 m between subarctic station K2 and subtropical station S1 based on drifting sediment trap experiments. J. Oceanogr. 72, 373–386. https://doi.org/10.1007/s10872-015-0280-x.
- Hu, D., Wu, L., Cai, W., Gupta, A.S., Ganachaud, A., Qiu, B., Gordon, A.L., Lin, X., Chen, Z., Hu, S., Wang, G., Wang, Q., Sprintall, J., Qu, T., Kashino, Y., Wang, F., Kessler, W.S., 2015. Pacific western boundary currents and their roles in climate. Nature 522, 299–308. https://doi.org/10.1038/nature14504.
- Hu, S., Sprintall, J., Guan, C., Sun, B., Wang, F., Yang, G., Jia, F., Wang, J., Hu, D., Chai, F., 2018. Spatiotemporal features of intraseasonal oceanic variability in the Philippine Sea from mooring observations and numerical simulations. J. Geophys. Res. Oceans 123, 4874–4887. https://doi.org/10.1029/2017JC013653.
- Hu, D., Wang, F., Sprintall, J., Wu, L., Riser, S., Cravatte, S., Gordon, A., Zhang, L., Chen, D., Zhou, H., Ando, K., Wang, Jianing, Lee, J.-H., Hu, S., Wang, Jing, Zhang, D., Feng, J., Liu, L., Villanoy, C., Kaluwin, C., Qu, T., Ma, Y., 2020. Review on observational studies of western tropical Pacific Ocean circulation and climate. J. Oceanol. Limnol. 38, 906–929. https://doi.org/10.1007/s00343-020-0240-1.
- Huang, J., Xu, F., 2018. Observational evidence of subsurface chlorophyll response to mesoscale eddies in the North Pacific. Geophys. Res. Lett. 45, 8462–8470. https://doi.org/10.1029/2018GL078408.
- Hung, C.-C., Gong, G.-C., Chung, W.-C., Kuo, W.-T., Lin, F.-C., 2009. Enhancement of particulate organic carbon export flux induced by atmospheric forcing in the subtropical oligotrophic northwest Pacific Ocean. Mar. Chem. 113, 19–24. https:// doi.org/10.1016/j.marchem.2008.11.004.
- Hwang, J., Manganini, S.J., Montluc, D.B., 2009. Dynamics of particle export on the Northwest Atlantic margin. Deep-Sea Res. I: Oceanogr. Res. Pap. 56, 1792–1803. https://doi.org/10.1016/j.dsr.2009.05.007.
- Ji, J., Ma, J., Dong, C., Chiang, J., Chen, D., 2020. Regional dependence of atmospheric responses to oceanic eddies in the north Pacific Ocean. Remote Sens. 12, 1161. https://doi.org/10.3390/rs12071161.
- Jiang, X., Dong, C., Ji, Y., Wang, C., Shu, Y., Liu, L., Ji, J., 2021. Influences of deep-water seamounts on the hydrodynamic environment in the northwestern Pacific Ocean. J. Geophys. Res. Oceans 126. https://doi.org/10.1029/2021JC017396.
- Jones, D.O.B., Yool, A., Wei, C., Henson, S.A., Ruhl, H.A., Watson, R.A., Gehlen, M.,
 2014. Global reductions in seafloor biomass in response to climate change. Glob.
 Chang. Biol. 20, 1861–1872. https://doi.org/10.1111/gcb.12480.
 Karl, D.M., Christian, J.R., Dore, J.E., Hebel, D.V., Letelier, R.M., Tupas, L.M., Winn, C.
- Karl, D.M., Christian, J.R., Dore, J.E., Hebel, D.V., Letelier, R.M., Tupas, L.M., Winn, C.D., 1996. Seasonal and interannual variability in primary production and particle flux at Station ALOHA. Deep Sea Res. Part II Top. Stud. Oceanogr. 43, 539–568. https://doi.org/10.1016/0967-0645(96)00002-1.
- Kawahata, H., Suzuki, A., Ohta, H., 2000. Export fluxes in the Western Pacific Warm Pool. Deep Sea Res. Part I Oceanogr. Res. Pap. 47, 2061–2091. https://doi.org/ 10.1016/S0967-0637(00)00025-X.
- Kiko, R., Biastoch, A., Brandt, P., Cravatte, S., Hauss, H., Hummels, R., Kriest, I., Marin, F., McDonnell, A.M.P., Oschlies, A., Picheral, M., Schwarzkopf, F.U., Thurnherr, A.M., Stemmann, L., 2017. Biological and physical influences on marine snowfall at the equator. Nat. Geosci. 10, 852–858. https://doi.org/10.1038/ psep3042
- Koppelmann, R., Weikert, H., Halsband-Lenk, C., Jennerjahn, T., 2004. Mesozooplankton community respiration and its relation to particle flux in the oligotrophic eastern Mediterranean: mesozooplankton community respiration. Glob. Biogeochem. Cycles 18, n/a-n/a. https://doi.org/10.1029/2003GB002121.
- Lampadariou, N., Tselepides, A., 2006. Spatial variability of meiofaunal communities at areas of contrasting depth and productivity in the Aegean Sea (NE Mediterranean). Prog. Oceanogr. 69, 19–36. https://doi.org/10.1016/j.pocean.2006.02.013.
- Lévy, M., Mémery, L., Madec, G., 1998. The onset of a bloom after deep winter convection in the northwestern Mediterranean Sea: mesoscale process study with a primitive equation model. J. Mar. Syst. 16, 7–21. https://doi.org/10.1016/S0924-7963(97)00097-3.
- Lins, L., Guilini, K., Veit-Köhler, G., Hauquier, F., Alves, R.M.S., Esteves, A.M., Vanreusel, A., 2014. The link between meiofauna and surface productivity in the Southern Ocean. Deep Sea Res Part II Top. Stud. Oceanogr. 108, 60–68. https://doi. org/10.1016/j.dsr2.2014.05.003.
- Longhurst, A.R., 2007. Ecological Geography of the Sea, Second edition. Academic Press.

- Lutz, M.J., Caldeira, K., Dunbar, R.B., Behrenfeld, M.J., 2007. Seasonal rhythms of net primary production and particulate organic carbon flux to depth describe the efficiency of biological pump in the global ocean. J. Geophys. Res. 112, C10011. https://doi.org/10.1029/2006JC003706.
- Ma, W., Xiu, P., Chai, F., Li, H., 2019. Seasonal variability of the carbon export in the central South China Sea. Ocean Dyn. 69, 955–966. https://doi.org/10.1007/s10236-019-01286-y
- Maier, S.R., Brooke, S., Clippele, L.H.D., de Froe, E., 2023. On the paradox of thriving cold-water coral reefs in the food-limited deep sea. Biol. Rev. https://doi.org/ 10.1111/bry.12976.
- Misic, C., Bavestrello, G., Bo, M., Borghini, M., Castellano, M., Covazzi Harriague, A., Massa, F., Spotorno, F., Povero, P., 2012. The "seamount effect" as revealed by organic matter dynamics around a shallow seamount in the Tyrrhenian Sea (Vercelli Seamount, western Mediterranean). Deep-Sea Res. I: Oceanogr. Res. Pap. 67, 1–11. https://doi.org/10.1016/j.dsr.2012.04.012.
- Ohman, M.D., Powell, J.R., Picheral, M., Jensen, D.W., 2012. Mesozooplankton and particulate matter responses to a deep-water frontal system in the southern California Current System. J. Plankton Res. 34, 815–827. https://doi.org/10.1093/ plankt/fbs028.
- Picheral, M., Catalano, C., Brousseau, D., Claustre, H., Coppola, L., Leymarie, E., Coindat, J., Dias, F., Fevre, S., Guidi, L., Irisson, J.O., Legendre, L., Lombard, F., Mortier, L., Penkerch, C., Rogge, A., Schmechtig, C., Thibault, S., Tixier, T., Waite, A., Stemmann, L., 2022. The Underwater Vision Profiler 6: an imaging sensor of particle size spectra and plankton, for autonomous and cabled platforms. Limnol. Oceanogr. Methods 20, 115–129. https://doi.org/10.1002/lom3.10475.
- Qin, X., Luo, W., Li, P., Chen, H., Xiao, X., Hu, G., Tan, Y., Du, R., Sun, M., Cong, J., Hu, X., Lu, K., Wang, L., Zhang, H., Zhou, H., 2021. Topographic and geomorphological features and tectonic genesis of the southern section of the Kyushu-Palau Ridge (KPR) and its adjacent areas. China Geol. 4, 1–14. https://doi.org/10.31035/cg2021076.
- R Core Team, 2022. R: A Language and Environment for Statistical Computing. R Foundation for Statistical Computing, Vienna, Austria.
- Ramondenc, S., Madeleine, G., Lombard, F., Santinelli, C., Stemmann, L., Gorsky, G., Guidi, L., 2016. An initial carbon export assessment in the Mediterranean Sea based on drifting sediment traps and the Underwater Vision Profiler data sets. Deep-Sea Res. I: Oceanogr. Res. Pap. 117, 107–119. https://doi.org/10.1016/j. dsr.2016.08.015.
- Ran, L., Chen, J., 2022. Sediment resuspension as a major contributor to sinking particles in the northwestern South China Sea: evidence from observations and modeling. Front. Mar. Sci. 9 https://doi.org/10.3389/fmars.2022.819340.
- Ruhl, H.A., Smith, K.L., 2004. Shifts in deep-sea community structure linked to climate and food supply. Science 305, 513–515. https://doi.org/10.1126/science.1099759.
- Shih, Y.-Y., Hung, C.-C., Gong, G.-C., Chung, W.-C., Wang, Y.-H., Lee, I.-H., Chen, K.-S., Ho, C.-Y., 2015. Enhanced particulate organic carbon export at eddy edges in the oligotrophic western North Pacific Ocean. PLoS One 10, e0131538. https://doi.org/ 10.1371/journal.pone.0131538.
- Siswanto, E., Ishizaka, J., Yokouchi, K., Tanaka, K., Tan, C.K., 2007. Estimation of interannual and interdecadal variations of typhoon-induced primary production: a case study for the outer shelf of the East China Sea. Geophys. Res. Lett. 34, L03604. https://doi.org/10.1029/2006GL028368.
- Smith, K.L., Ruhl, H.A., Kahru, M., Huffard, C.L., Sherman, A.D., 2013. Deep ocean communities impacted by changing climate over 24 y in the abyssal northeast Pacific Ocean. Proc. Natl. Acad. Sci. 110, 19838–19841. https://doi.org/10.1073/ pnas.1315447110.
- Stemmann, L., Picheral, M., Gorsky, G., 2000. Diel variation in the vertical distribution of particulate matter (>0.15 mm) in the NW Mediterranean Sea investigated with the Underwater Video Profiler. Deep-Sea Res. I: Oceanogr. Res. Pap. 47, 505–531. https://doi.org/10.1016/S0967-0637 (99)00100-4.
- Stemmann, L., Eloire, D., Sciandra, A., Jackson, G.A., Guidi, L., Picheral, M., Gorsky, G., 2008a. Volume distribution for particles between 3.5 to 2000 μm in the upper 200 m region of the South Pacific Gyre. Biogeosciences 5, 299–310.

- Stemmann, L., Hosia, A., Youngbluth, M.J., Søiland, H., Picheral, M., Gorsky, G., 2008b. Vertical distribution (0–1000 m) of macrozooplankton, estimated using the Underwater Video Profiler, in different hydrographic regimes along the northern portion of the Mid-Atlantic Ridge. Deep Sea Res. Part II Top. Stud. Oceanogr. 55, 94–105. https://doi.org/10.1016/j.dsr2.2007.09.019.
- Sugimoto, T., Tadokoro, K., 1998. Interdecadal variations of plankton biomass and physical environment in the North Pacific. Fish. Oceanogr. 7, 289–299. https://doi. org/10.1046/j.1365-2419.1998.00070.x.
- Sweetman, A.K., Thurber, A.R., Smith, C.R., Levin, L.A., Mora, C., Wei, C.-L., Gooday, A. J., Jones, D.O.B., Rex, M., Yasuhara, M., Ingels, J., Ruhl, H.A., Frieder, C.A., Danovaro, R., Würzberg, L., Baco, A., Grupe, B.M., Pasulka, A., Meyer, K.S., Dunlop, K.M., Henry, L.-A., Roberts, J.M., 2017. Major impacts of climate change on deep-sea benthic ecosystems. Elem. Sci. Anthr. 5, 4. https://doi.org/10.1525/elementa.203.
- Tittensor, D.P., Rex, M.A., Stuart, C.T., McClain, C.R., Smith, C.R., 2011. Species–energy relationships in deep-sea molluscs. Biol. Lett. 7, 718–722. https://doi.org/10.1098/rsbl.2010.1174.
- Turner, J.T., 2015. Zooplankton fecal pellets, marine snow, phytodetritus and the ocean's biological pump. Prog. Oceanogr. 130, 205–248. https://doi.org/10.1016/j.pocean_2014_08_005
- Turnewitsch, R., Dumont, M., Kiriakoulakis, K., Legg, S., Mohn, C., Peine, F., Wolff, G., 2016. Tidal influence on particulate organic carbon export fluxes around a tall seamount. Prog. Oceanogr. 149, 189–213. https://doi.org/10.1016/j.pocean_2016_10_009
- Van Haren, H., Millot, C., Taupier-Letage, I., 2006. Fast deep sinking in Mediterranean eddies. Geophys. Res. Lett. 33, L04606. https://doi.org/10.1029/2005GL025367.
- Waite, A.M., Stemmann, L., Guidi, L., Calil, P.H.R., Hogg, A.M.C., Feng, M., Thompson, P.A., Picheral, M., Gorsky, G., 2016. The wineglass effect shapes particle export to the deep ocean in mesoscale eddies. Geophys. Res. Lett. 43, 9791–9800. https://doi.org/10.1002/2015GL066463.
- Wang, L., Huang, B., Laws, E.A., Zhou, K., Liu, X., Xie, Y., Dai, M., 2018. Anticyclonic eddy edge effects on phytoplankton communities and particle export in the northern South China Sea. J. Geophys. Res. Oceans 123, 7632–7650. https://doi.org/ 10.1029/2017JC013623.
- Wei, C.-L., Rowe, G.T., Escobar-Briones, E., Boetius, A., Soltwedel, T., Caley, M.J., Soliman, Y., Huettmann, F., Qu, F., Yu, Z., Pitcher, C.R., Haedrich, R.L., Wicksten, M. K., Rex, M.A., Baguley, J.G., Sharma, J., Danovaro, R., MacDonald, I.R., Nunnally, C. C., Deming, J.W., Montagna, P., Lévesque, M., Weslawski, J.M., Wlodarska-Kowalczuk, M., Ingole, B.S., Bett, B.J., Billett, D.S.M., Yool, A., Bluhm, B.A., Iken, K., Narayanaswamy, B.E., 2010. Global patterns and predictions of seafloor biomass using random forests. PLoS One 5, e15323. https://doi.org/10.1371/journal.pone.0015323.
- Wolff, G.A., Billett, D.S.M., Bett, B.J., Holtvoeth, J., FitzGeorge-Balfour, T., Fisher, E.H., Cross, I., Shannon, R., Salter, I., Boorman, B., King, N.J., Jamieson, A., Chaillan, F., 2011. The effects of natural iron fertilisation on deep-sea ecology: the Crozet Plateau, Southern Indian Ocean. PLoS One 6, e20697. https://doi.org/10.1371/journal.pone.0020697.
- Zhou, K., Dai, M., Kao, S.-J., Wang, L., Xiu, P., Chai, F., Tian, J., Liu, Y., 2013. Apparent enhancement of ²³⁴Th-based particle export associated with anticyclonic eddies. Earth Planet. Sci. Lett. 381, 198–209. https://doi.org/10.1016/j.epsl.2013.07.039.
- Zhou, K., Dai, M., Maiti, K., Chen, W., Chen, J., Hong, Q., Ma, Y., Xiu, P., Wang, L., Xie, Y., 2020. Impact of physical and biogeochemical forcing on particle export in the South China Sea. Prog. Oceanogr. 187, 102403 https://doi.org/10.1016/j.pocean.2020.102403.
- Zhou, K., Benitez-Nelson, C.R., Huang, J., Xiu, P., Sun, Z., Dai, M., 2021. Cyclonic eddies modulate temporal and spatial decoupling of particulate carbon, nitrogen, and biogenic silica export in the North Pacific Subtropical Gyre. Limnol. Oceanogr. 66, 3508–3522. https://doi.org/10.1002/lno.11895.